

UCSF

UC San Francisco Electronic Theses and Dissertations

Title

Mechanisms of Kinesin Processivity

Permalink

<https://escholarship.org/uc/item/17c615bv>

Author

Jonsson, Erik

Publication Date

2015

Peer reviewed|Thesis/dissertation

Mechanisms of Kinesin Processivity

by

Erik Jonsson

DISSERTATION

Submitted in partial satisfaction of the requirements for the degree of

DOCTOR OF PHILOSOPHY

in

Biophysics

in the

GRADUATE DIVISION

of the

UNIVERSITY OF CALIFORNIA, SAN FRANCISCO

Copyright (2015)

by

Erik Jonsson

*Dedicated to my father, who always
discussed science with me*

Acknowledgements

I believe that no meaningful endeavor can be accomplished without the help and support of others. As such, I would like to take this opportunity thank many people for their help and support. First and foremost, I would like to thank Ron Vale, my thesis advisor. Without him none of this would have been possible but, more importantly, he helped me transition from being a ‘good student of science’ to being a ‘good scientist’. He has been a great mentor and I am extremely grateful. Also, Phoebe Grigg, Nan Zhang, and Nico Stuurman have helped in countless ways along the course of my PhD. Thank you as well to the tireless work Rebecca Brown on my behalf. The entire members of the Vale lab but especially members of Bay 4 – Sarah Goodwin, Melissa Hendershott, Thomas Huckaba, Susana Ribeiro, Yuxiao Wang, and Garrett Greenan (alternate bay 4 member). Also, thanks to the other members of the lab: Sabine Petry, Eric Griffis, Gira Bhabha, Damien Ekiert, Marcus Taylor (also should probably mention Tonto and Tesla), Rick McKenny, and Kassandra Ori-McKenney (honorary Vale lab member), Adam Williamson, Courtney Schroeder, Xialoei Su, Ankur Jain. Also, a special thank you to my tennis partner Enfu Hui – although he has taken a fourteen year break from tennis, he was always willing to help me with science. And to the rest of the Vale lab family, both new and old, (some of whom I may have forgotten to mention) are all great people and I’ve enjoyed working with them.

UCSF was a fantastic place to work. I've made some great friends along the way – Charles Greenberg and Peter Cimermanic (true 'gentlemen scientists'). It was always fun to chat with Aram Avila-Herrera and Jonathan Gable, especially after long days in the lab. Other members of our cohort Si-Han Chen, Zhiyuan Li, and Laurens Kraal were also fun people to run into in the halls. Also, there are countless members of the UCSF community whom I would like to thank and so I will just list them in no particular order: Daniel Elnatan, David Booth, Stephen Floor, Emmanuel Yera, Rebeca Choy, Jonathan Ostrem, Charles Morgan, Dan Gray and countless others from the UCSF community. Also, thank you to the Woods hold community.

I would like to thank my thesis committee – Robert Fletterick, Bo Huang and Jamie Fraser – who, besides being great scientists, are simply great people. Mentorship comes in a variety of forms at UCSF and I've received my fair share. Thanks to Joe Derisi, with his commitment such things as 'team challenge', which stand out among my happiest memories at UCSF. Thank you to John Gross (my interview with him was a deciding factor to come to UCSF) and Ajay Jain. Thank you to Jim Wells, Peter Walter and Ciara Gallagher. Thank you to my original mentors in the Vale lab – Arne Gennerich, Andrew Carter and Minhaj Sirajuddin. Thank you to Jim Hartman, Ed Taylor and my collaborators: Gohta Goshima, Moe Yamada, Michio Tomishige, Yamato Niitani.

Lastly I would like to thank my family. Thank you to my mom, and golf buddy, who listened to me through all the ups and downs. Thank you to my dad, who afforded me the opportunity to be able to pursue a PhD. Thank you to my two sisters Kika and Alicia, whom I love very much. And last but certainly not least, thank you my kind, beautiful, loving and supportive wife Yulia – I think she deserves an honorary degree solely for supporting me through this process. Thank you all.

Contributions

Chapter II of this thesis is a reprint of the material as it appears in:

Jonsson, E., Yamada, M., Vale, R.D., Goshima G.(2015) *Clustering of a kinesin-14 motor enables processive retrograde microtubule-based transport in plants*. **Nature Plants 1: 1-7**.

The co-authors Moe Yamada and Gohta Goshima are collaborators who provided support in the form of *in vivo* experiments which were incorporated into the paper. The bulk of Erik Jonsson's experimental work (all *in vitro* experiments as described in the methods section) was carried out under the supervision of Ronald D. Vale. Erik Jonsson wrote the manuscript with input and supervision from both Ronald D. Vale and Gohta Goshima.

Abstract

Kinesins are molecular motors that convert chemical energy, stored in the bonds of ATP, into productive work. They form one of the three branches of cytoskeletal motors – the others being myosins and dyneins. An important subset of molecular motors, in general, are transport motors. By utilizing microtubule filaments as their track, these protein machines shuttle cargo to different destinations within a cell. *Processivity*, the ability to take multiple ATP-dependent steps along the filament, is an essential characteristic of these transport motors. In this dissertation I explore two distinct mechanisms of kinesin processivity. Previously, the only known mode of processive retrograde microtubule-based transport is achieved via cytoplasmic dynein. Land plants are thought to have lost the gene encoding for cytoplasmic dynein and thus, as of 2012, it was an open question as to whether they relied at all on microtubule based transport. In the first part of this dissertation, I discuss a novel mechanism of processive retrograde microtubule-based transport in *Physcomitrella patens* (moss). A kinesin-14 motor protein was found to be capable of processively transporting cargo when the motors are clustered together in small cohorts. In the second part, I explore the processivity of kinesin-1, one of the most well-studied molecular motors. Its processivity is known to be due to an allosteric mechanism, referred to as *gating*, but the nature of the mechanism has remained elusive. The precise gating mechanism of

kinesin-1 has been heavily debated in the thirty years since its discovery. By combining modern protein purification techniques with a classical pre-steady state kinetics approach, I demonstrate that the prominent front head gating model, in its current form, is incorrect and needs to be revised.

Table of Contents

Preface	Acknowledgements	iv
	Contributions	vii
	Abstract	viii
	List of Tables	xi
	List of Figures	xii
Chapter 1	Introduction	1
Chapter 2	Kinesin-14 Retrograde Transport in Moss	11
Chapter 3	Kinesin-1 Gating	54
Chapter 4	In Conclusion	74

List of Tables

Table S1: List of PCR Primers used in this study	38
Table 1: Steady state ATPase data	63

List of Figures

Chapter II

Figure 1. Four kinesin-14 subgroup members exhibit minus-end-directed motor activity	16
Figure 2. Artificially tetramerized kin14-VIb showed processive motility . . .	20
Figure 3. Kin14-VIb transports liposomes along MTs	24
Figure 4. Minus-end-directed motility of kin14-VIb clusters <i>in vivo</i>	27
Supplementary Figure S1. Additional <i>P. patens</i> kinesin-14 characterization . .	32
Supplementary Figure S2. Kin14-VIb full-length is non-processive on its own, but transports liposomes for long distance	34
Supplementary Figure S3. Establishment of the kin14-VIb replacement line .	36

Chapter III

Figure 1. Mant-nucleotide binding to microtubule-bound monomeric kinesin constructs	57
Figure 2. Kinesin heterodimer kinetic measurements	60
Figure 3. Phosphate release kinetics	66

Chapter IV

Figure 1. Model for kinesin front head gating mechanism.	80
--	----

Chapter I

Introduction

Cells are often described as cities bustling with enzymes performing the various tasks necessary to sustain life. This analogy is appealing for a variety of reasons. Imagine that if we were tasked with understanding how a city works, say for example San Francisco, it would be impossible to undertake such a challenge head on. We might have to start by narrowing our focus down to a particular neighborhood or street, getting to know the architecture and the people who inhabit it, observing their activities that can later be codified into patterns. The same is true of biology - when faced with the scale and complexity of the system, we must narrow our focus. One way, is to concentrate onto a class of enzymes known as *molecular motors*, which generate work from stored potential energy. In keeping with the previous analogy, a city is filled with machines that consume energy to produce work: large cranes, automobiles, elevators, to name a few. We can subdivide these machines into those that utilize the infrastructure of a city (streets, train tracks, waterways, etc...) for *transport*. These transport machines are incredibly diverse, from the cars that commute in and out of the city, to the cargo ships that transport goods from other continents, to the cable cars on Powell street. But in spite of such diversity we can deduce general principles. For example, if we concern ourselves with how a particular car engine works, we might then be able to infer more general properties governing the function of the combustion engine, which would be

applicable to a larger class of machines. Similarly by focusing our attention on a few molecular motor prototypes we can infer general properties of a larger class of proteins. The narrowing of focus for our purposes proceeds as follows. Molecular motors can be subdivided into *cytoskeletal motors* which can further be subdivided into *transport motors*. The principles that govern the function of two prototypical transport motors are what forms the basis of this thesis.

The cytoskeleton provides structural support to a cell predominantly in the form of actin filaments and microtubules. The importance of the cytoskeleton cannot be overstated. It is a distinguishing characteristic that sets higher organisms apart from prokaryotes. Motors have evolved to both utilize and shape the cytoskeleton for various purposes. Large morphological changes to a cell, such as mitosis or neuronal differentiation, necessarily involve cytoskeletal motors. Three families of cytoskeletal motors have been discovered: Myosins, Kinesins and Dyneins. All three families contain motors that transport cargo (collections of macromolecules), shuttling them from one place to another within a cell. To understand the importance of such behavior, consider the following example. The shape of a neuron differs dramatically than that of a more common compact cell shape. From the perspective of a single protein of average size ($\sim 10^{-9}$ m), the distance from the nucleus to the distal axonal tip is enormous and can be as large as 1 meter. Given that the nucleus (the factory that

produces macromolecules) is so far removed from the tip of the axon (a site that requires them) presents a conundrum – how do these molecules make it to their destination? The time for diffusion along the length of the axon is astronomical. Kinesin-1, a transport motor, solves this problem by utilizing a network of polarized microtubules that span the length of the corridor, from the nucleus to the axonal tip. By converting the energy stored in the chemical bonds of ATP, kinesin shuttles its cargo along the length of the axon thereby overcoming a significant barrier imposed by diffusion.

There are many questions we might ask about how such transport motors work. We can ask questions at the genetic level about regulation or we might inquire about how cargo is selected but our focus here will be on how they move. We can look under the hood of a car to observe how the pistons move in response to fuel combustion, and by analogy we would like to know what are the mechanistic details about how kinesin utilizes its energy source (ATP) to move along a microtubule. In other words, what are the precise events along the kinesin cycle that result in directed motion? Additionally a hallmark of transport motors is that they are generally *processive*. A delivery truck that is constantly driving off the road or getting lost down side streets would not be very effective at its task and would consume much precious fuel in the process. Similarly for kinesin-1, it has been known for quite some time that there is a mechanism

responsible for keeping it engaged with the microtubule (referred to as gating), on its track and preventing it from diffusing away. As will be discussed later, processivity is a feature that makes the motors amenable to single molecule observation in a microscope. But, rather than being simply an academic curiosity, processivity is a fundamental property that facilitates transport along cytoskeletal filaments. It is necessary by virtue of having to operate in a Brownian environment. This thesis is separated into two parts that deal with distinct mechanisms of processivity in different contexts.

Part I is a project that arose out of the observation that plant genomes lack cytoplasmic dynein. This is true for all land plants, such as the model organisms rice, maize, *Arabidopsis* and *Physcomitrella Patens* (moss). As an aside, for a brief period it was reported that rice contained dynein but it was later revealed to be an artifact, due to contamination, in the sequencing process. At the time of embarking on this project (summer 2012) it was generally accepted that land plants had lost dynein in the course of their evolutionary history. Recall, that dyneins form one of the three families of cytoskeletal motors. Unlike myosins and kinesins, however, which are often present in abundance, animal genomes tend to have only one or two dyneins. And these genes are essential, critical for processes like mitosis. The immediate question that arises is how do plants cope without this motor, which is fundamentally important in almost all

other studied Eukaryotes? In other studied Eukaryotic systems dynein is the only mode of *retrograde* transport – i.e. transport towards the minus end of the microtubule. At the time of publication, all known kinesin transport was exclusively *anterograde* – i.e. move towards the plus end. Plant genomes have plenty of kinesin genes but how could they survive with only the ability to transport in one direction along the microtubule? One theory was that plants simply do not rely on the microtubule cytoskeleton for transport. That is, all transport needs are fulfilled by myosin motors interacting with actin (as is the case in cytoplasmic streaming). Plant biology is drastically different than animal biology and this hypothesis is certainly plausible. But closer inspection reveals a curious feature that plant genomes tend to have an expanded set of kinesin-14s, in fact many more than animals. Though never implicated as transport motors, kinesin-14s are critically important in animal biology and do exhibit retrograde polarity. Thus we embarked on this project by asking the question, *are any of these plant kinesin 14s processive retrograde transporters?*

Operating on the assumption that if plants have genes encoding for anterograde transport motors (as they do) then they must surely have one, or more, encoding for retrograde transport. Therefore, this project was more exploratory and, as such, we did not know what we would find. We attempted to cast as wide a net as possible while putting ourselves in a position to observe novel biology. We did not find a processive

motor as we had expected but, instead, we found evidence that supports a completely novel mechanism of retrograde transport. This also leads us to believe that plant biology houses vast undiscovered territory.

Another important aspect of this project is that it embodies a distinct personality, sort of an ambitious and collegial spirit of discovery, that persists at the MBL (Marine Biological Laboratory) in Woods Hole, MA – where we began the project in 2012. Every summer scientists from all over the world meet at Woods Hole to engage in scientific discussions and experimental inquiry. It is out of this space, carved out for riskier but potentially more fruitful discoveries, where both projects originated. It was 30 years ago that kinesin-1 was discovered at the MBL.

Part II is a story about kinesin-1. Unlike the kinesin-14s in part I, kinesin-1 has been studied extensively in the decades since its discovery. Interest in this motor is due in large part because it serves as one of the main prototypes for understanding how *all* molecular motors work. Again, here we focus on the nature of processivity and the mechanism is quite different than the one we propose in part I. To understand the distinction consider the following analogies. Imagine a millipede might crawling along a twig. It does not fall off due to a ‘safety in numbers’ approach. It has many legs that are attached at any given time to the twig that it need not regulate the activity of each

individual leg. Even if it were to flail its legs stochastically, it would not fall off due to the high probability that when one leg is detached there are many others still stuck to the twig. Alternatively consider how an ape swings along a vine. The ape doesn't have the same luxury as the millipede because it only has a few limbs that can engage with the vine. Instead he must coordinate the activity of his motion and make sure that at least one limb is securely attached to the vine at all times. Thus this model is more of a 'coordination' approach to processivity.

Embarking on the question of kinesin-1 processivity did not afford us the same freedom we had in part I, as attempts to elucidate the nature of its processivity is a well-trodden path. Much is known about how kinesin-1 functions and decades of study on the mechanism necessarily forced us to focus on very nuanced aspects of its kinetic cycle. In particular, just as the ape makes sure that at least one limb is attached to the vine at all times, so too does kinesin coordinate its interactions with the microtubule. It has been known for nearly as long as it has been studied that kinesin-1 is a dimer, with two catalytic sites that do not operate independently. Rather than cycling stochastically, the two catalytic protomers coordinate their activity via a mechanism known as *gating*. Many gates have been proposed but it is still an open question.

Another major difference between part I and part II is in the experimental approach. In a sense our hand was forced as there had already been numerous single molecule studies on kinesin-1. Arguably this protein is responsible for numerous advances in single molecule techniques and advanced microscopy. This is no surprise as there is a symbiosis between biological questions we ask and the tools we use to answer them. When faced with a boundary of what we can measure we develop a novel approach to inquire more deeply. This new technique might answer our question but will inevitably lead to new questions with new boundaries requiring a novel approach, and so on. Thus advances in microscopy and our understanding of biological systems proceed in parallel. As an example, it was thought for a long time that the diffraction limit set a lower bound on what could be resolved in a microscope. But transformative approaches to blow past this limit have resulted in a Nobel prize awarded last year.

The problem as we saw it, however, was not a lack of techniques available but, rather, that the field had converged on a single style of experimental inquiry. Almost, all of the studies aimed at addressing the question of kinesin processivity were single molecule studies. These approaches have been invaluable and led to deep understanding of the kinesin-1 mechanism but were fundamentally ill-suited to resolving this question. We therefore decided to take a step back and approach this problem from a different perspective. As will be described in part II, the prominent gating model that emerged

from single molecule studies was one in which gating occurs at the level of ATP binding. As no single molecule experiment has been able to satisfactorily measure directly how this process occurs, we thought we had an opening. We designed an approach based on modern protein purification techniques but in the context of classical kinetic methodologies. The appeal being that we could test this hypothesis directly, without model based assumptions that have plagued many previous studies. What we found that our evidence did not support the model which had gained favor in the field recently. Therefore, we challenge the current gating hypothesis and offer a different model in its place.

Chapter II

Retrograde Transport in Moss

Clustering of a kinesin-14 motor enables processive retrograde microtubule-based transport in plants

Erik Jonsson ^{1,2}, Moé Yamada ^{1,3}, Ronald D. Vale ^{1,2}, and Gohta Goshima ^{1,3†}

¹Marine Biological Laboratory, Woods Hole, MA 02543, USA

²Howard Hughes Medical Institute and Department of Cellular and Molecular Pharmacology, UCSF, 600 16th St., San Francisco, USA

³Division of Biological Science, Graduate School of Science, Nagoya University, Furo-cho, Chikusa-ku, Nagoya 464-8602, Japan

The molecular motors kinesin and dynein drive bidirectional motility along microtubules (MTs) in most eukaryotic cells^{1,2}. Land plants, however, are a notable exception, since they contain a large number of kinesins but lack cytoplasmic dynein, the foremost processive retrograde transporter^{3,4}. It remains unclear how plants achieve retrograde cargo transport without dynein. Here, we have analyzed the motility of the six members of minus-end-directed kinesin-14 motors in the moss *Physcomitrella patens* and found that none are processive as native dimers. However, when artificially clustered into as little as dimer of dimers, the type-VI kinesin-14 (a homologue of *Arabidopsis* KCBP [kinesin-like calmodulin binding protein]) exhibited highly processive and fast motility (up to 0.6 $\mu\text{m/s}$). Multiple kin14-VI dimers attached to liposomes also induced transport of this membrane cargo over several microns. Consistent with these results, *in vivo* observations of GFP-tagged kin14-VI in moss cells revealed fluorescent punctae that moved processively towards the minus ends of the cytoplasmic MTs. These data suggest that clustering of a kinesin-14 motor serves as a dynein-independent mechanism for retrograde transport in plants.

Organelle transport in plant cells has generally been considered to be actin and myosin dependent (e.g. cytoplasmic streaming)⁵. However, MT-based motility has also been observed in some plant systems and is plausibly dependent on kinesin, another class of cytoskeletal motor⁵⁻⁸. Kinesins constitute a large superfamily, the founding member of which (kinesin-1) forms homodimers that take many steps along a MT towards the plus end before dissociating¹. Such processive movement allows this kinesin to function efficiently in the long distance anterograde transport of cargo. Within the kinesin superfamily, the kinesin-14 motors are distinct from other kinesin families in that they display minus-end-directed movement, and are therefore potential retrograde transporters⁹. Recently, Kar3, an atypical kinesin-14 present in budding yeast, was shown to move processively towards minus-ends via heterodimerization with a non-motor subunit^{10,11}. However, none of the animal or plant kinesin-14s characterized to date, which form homodimers, have shown fast and processive motility. The best-studied protein is Ncd, the sole kinesin-14 member in *Drosophila*, which exhibits short residency times that coincide with the length of time it takes to bind and hydrolyze ATP¹². Ncd is required for mitotic and meiotic spindle MT crosslinking, but is sequestered in the nucleus in interphase^{13,14}; thus, it is unlikely that Ncd plays a major role in cargo transport in the interphase cytoplasm. In plants, kinesin-14 genes have been heavily duplicated, and there are 21 and 15 genes in the seed plant *Arabidopsis* and

the moss *Physcomitrella patens*, respectively^{15,16}. Some kinesin-14 members appear to have non-mitotic roles, such as KCBP in trichome morphogenesis¹⁷ and the KCA/KAC kinesin in positioning of the chloroplast in the cytoplasm^{18,19}. It is unknown if any members of the kinesin-14 subfamily in plants are capable of processive motility and/or are involved in MT-based cargo transport.

Fifteen kinesin-14s of *P. patens* are further subdivided into six subgroups, based on the amino acid sequence similarity of the motor and the adjacent neck domains (Fig. 1a)¹⁵. Within these subgroups, the amino acid sequences are very similar to each other (e.g., kin14-Ia and -Ib share nearly 87% sequence identity) and are therefore thought to function redundantly, as was previously shown for the kin14-V proteins¹⁸. On the other hand, the lengths, sequences and domain organization are markedly different between the subgroups (Fig. 1a). To test if any of the kinesin-14 motors show processive minus-end-directed motility, we selected one representative member from each of the six protein subgroups for biochemical analysis. Characterization of kinesins has generally been achieved with truncated constructs in which the neck and motor domains are included. We therefore engineered truncations of Ppkinesin-14s fused with an N-terminal GFP (Fig. 1b). Gel filtration chromatography showed that they eluted at a similar fraction to a dimeric Ncd motor construct (236–700 a.a., tagged with GFP), suggesting that they are also dimeric (Fig. S1b).

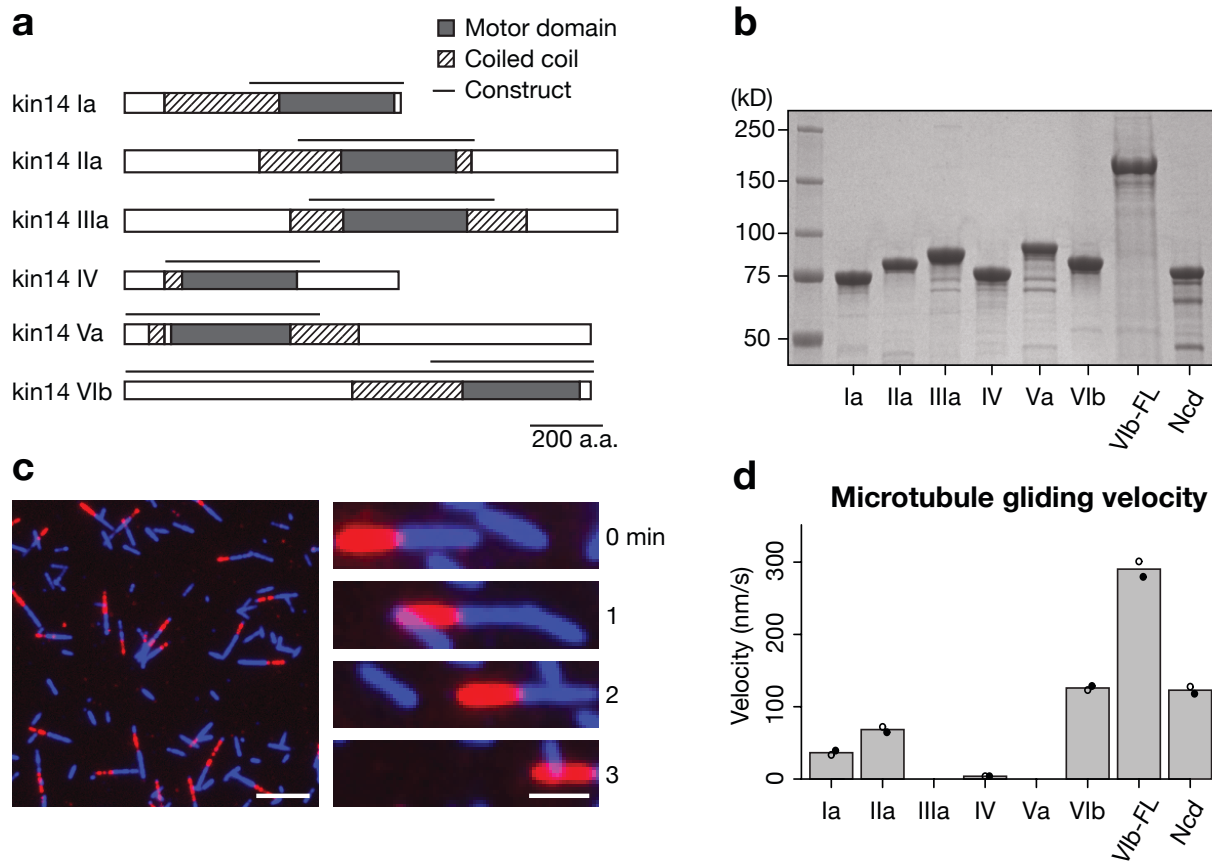


Figure 1. Four kinesin-14 subgroup members exhibit minus-end-directed motor activity

(a) Gene maps of the six subgroups of kinesin-14s in *Physcomitrella patens*. (b) Coomassie blue staining after SDS-PAGE of the purified proteins used in the motility assays (FL stands for full-length). (c) An example of a gliding assay used to determine motor velocity and directionality (in this case kin14-Ia). MT minus ends are labeled in red. Bar, 5 μm (left) or 2 μm (right). (d) Gliding velocities. Bars represent the mean

velocity of two independent experiments utilizing different protein purifications; solid and filled circles show the results from each preparation. Each circle represents the mean velocity of at least 100 motile MTs.

The purified proteins were assayed for motility in a MT gliding assay, in which motors were adhered to a cover glass and then MTs and ATP were added to the reaction chamber. Four of the six truncated chimeras translocated MTs with velocities ranging from 4–130 nm/s (Fig. 1d, Movie 1). The fastest motor (kin14-VIb) showed a gliding velocity similar to Ncd and KCBP²⁰. Kin14-IIIa did not translocate MTs along the glass surface, although they bound to MTs in an ATP-dependent manner in a sedimentation assay (Fig. S1c). Kin14-Va did not efficiently bind to MTs, consistent with its *Arabidopsis* orthologue (Fig. S1c)¹⁸. To determine the directionality of the moving MTs, we also performed a gliding assay with polarity marked MTs (Fig. 1c). As the MTs predominantly moved with their plus ends leading (Fig. S1a), we concluded that the four motile kinesin-14 subgroups are all minus-end-directed motors.

We asked whether any of the active motors might also be processive in a single molecule motility assay. This assay involves attaching MTs to a coverslip and then adding low levels of GFP-tagged kinesin to examine the interactions of single motors with MTs. We performed this assay with high (2 mM) and low (10 μ M) concentrations of ATP, but did not observe processive motion for any construct (Fig. 2a shows a representative kymograph for kin14-VIb).

We measured gliding velocity as a function of surface motor density for kin14-VIb (Fig. S2a). The velocity was insensitive to a wide range of surface densities. However, at low surface densities (less than approximately 1 molecule/ μm^2), MTs attached to the surface but no longer exhibited unidirectional motion. The gliding velocity decreased slightly for the two highest surface density measurements, indicating that the motors can interfere with each other when present in sufficiently high numbers.

We then wondered if the full-length proteins might contain some additional domain that confers processivity. We therefore expressed full-length versions of the two fastest motors (kin14-IIa and -VIb). While we failed to purify full-length kin14-IIa after several attempts, we successfully purified the full-length kin14-VIb (kin14-VIb FL) (Fig. 1b). Kin14-VIb FL showed minus-end-directed MT gliding activity, and the gliding velocity was faster than the truncated form (~ 300 nm/s; Fig. 1d). To test if the increase in velocity is due to higher ATPase rate of the FL, we measured the steady-state ATPase activity of truncated and FL constructs (Fig. S2b). The truncated kin14-VIb had a similar rate to those previously reported for Ncd^{21,22}. However, the rate was ~ 10 -fold lower for the FL. A likely interpretation of this data is that the full-length protein in solution is in an auto-inhibitory form with a low ATPase rate, as is well-documented for kinesin-1 and other anterograde kinesin motors²³. We speculate that the overall protein size affects its velocity, as is the case for Ncd²². Although it

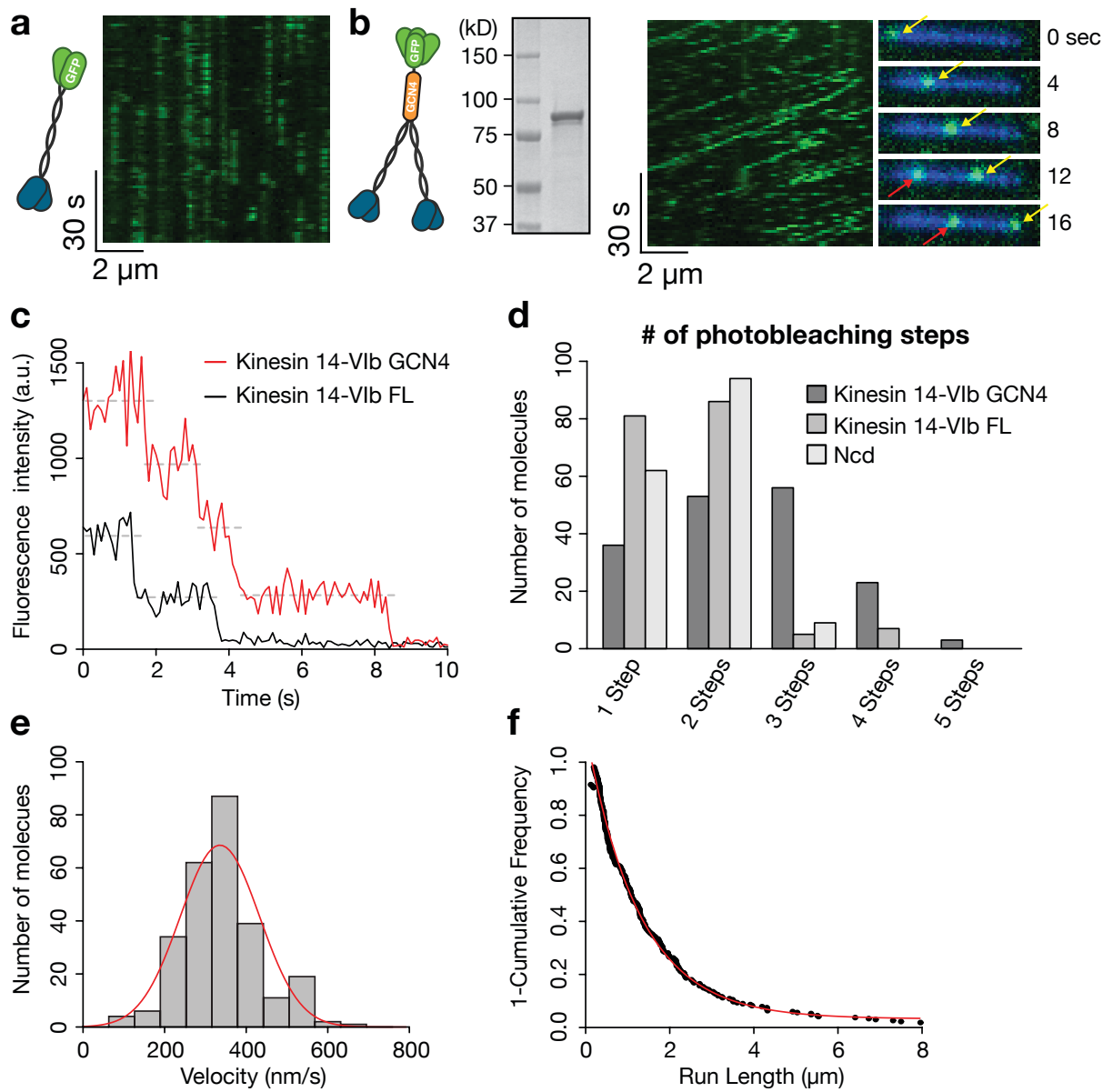


Figure 2. Artificially tetramerized kin14-VIb showed processive motility

- (a) A kymograph for dimeric kin14-VIb motors reveals no processive movement.
- (b) A kymograph for the GFP-kin14-VIb GCN4 tetramer construct exhibits clear processive movement (diagonal lines) and long run lengths. Movie frames show

two separate GFP spots (arrows), moving along a MT (blue). (c) Representative traces of the photobleaching of kin14-VIb FL and the kin14-VIb GCN4 tetramer. (d) Quantitation of the number of photobleaching steps. (e) Velocity histogram of the kin14-VIb GCN4 tetramer with mean of 336 ± 97 nm/s (mean \pm SD, n = 267). (f) 1-Cumulative frequency for run lengths of the GCN4 tetramer construct, which were fit to an exponential yielding a fit parameter of $\lambda = 1.27 \pm 0.03$ μ m (error was determined from goodness of fit parameters; $R^2 = 0.995$, n = 267 particles).

translocated MTs at faster rate, the full-length, dimeric proteins were still non-processive in the single molecule motility assay (Fig. S2c). On rare occasions, we observed a GFP particle that moved processively (Fig. S2c). However, these motile particles were significantly brighter than the non-motile particles, suggesting that they are small aggregates and not single native dimers.

These results suggested that a small cohort of kin14-VIb motors could potentially move processively. We therefore engineered the “dimer of dimers” construct by introducing the coding sequence for a GCN4 parallel tetramer motif²⁴ into the N-terminus (Fig. 2b). To confirm that the kin14-VIb GCN4 construct is indeed a tetramer, we measured its photobleaching characteristics (Fig. 2c, d). Fig. 2c compares representative traces for kin14-VIb GCN4 and dimeric kin14-VIb FL, which showed 4- and 2-step photobleaching processes, respectively. The observed photobleaching step distribution of kin14-VIb GCN4 (n = 199) was distinct from that of dimeric Ncd or kin14-VIb FL (Fig. 2d), and was more consistent with that of other tetrameric proteins analyzed in a similar manner²⁵. Prevalence of ≤ 3 bleaching steps over 4 steps in the tetramer is likely due to GFP photo-inactivation prior to image acquisition, as is commonly reported²⁶. Taken together, we conclude, as expected, that kin14-VIb GCN4 is tetrameric, while kin14-VIb FL, like Ncd, is dimeric.

In the single molecule motility assay, kin14-VIb GCN4 exhibited frequent processive motility (Fig. 2b, Movie 2). The velocity was 336 ± 97 nm/s, which was significantly higher than its gliding velocity of 125 nm/s (Fig. 1d). Kin14-VIb GCN4 exhibited long run lengths of 1.27 ± 0.03 μ m, (exponential fit parameter \pm error of fit, $R^2 = 0.995$), which is comparable to the run length of human kinesin-1 processivity *in vitro* (Fig. 2f)²⁷. When we attached the GCN4 tetramer motif to kin-14IIa, the second fastest kin14 (Fig. 1d), we did not observe processive motion (Fig. S2d). We therefore focused on kin-14VIb for further characterization.

As an alternative *in vitro* clustering assay, we adhered multiple kin14-VIb motors to liposomes. To this end, we assembled liposomes with incorporated DOGS-NTA-Ni lipids, such that multiple histidine-tagged kin14-VIb proteins could bind to the liposomes (Fig. 3a and S2e). The liposomes were transported along MTs for long distances (Fig. 3b, c, Movie 3). Some moving liposomes switched between MT tracks, indicating that multiple motors were indeed present on their surface. The velocities (266 ± 69 nm/s for kin14-VIb and 597 ± 134 nm/s for kin14-VIb FL; Fig. 3d) were twice as fast as the gliding velocities, and the FL transport length was several microns, which is comparable to mammalian dynein²⁸ (Fig. S2f).

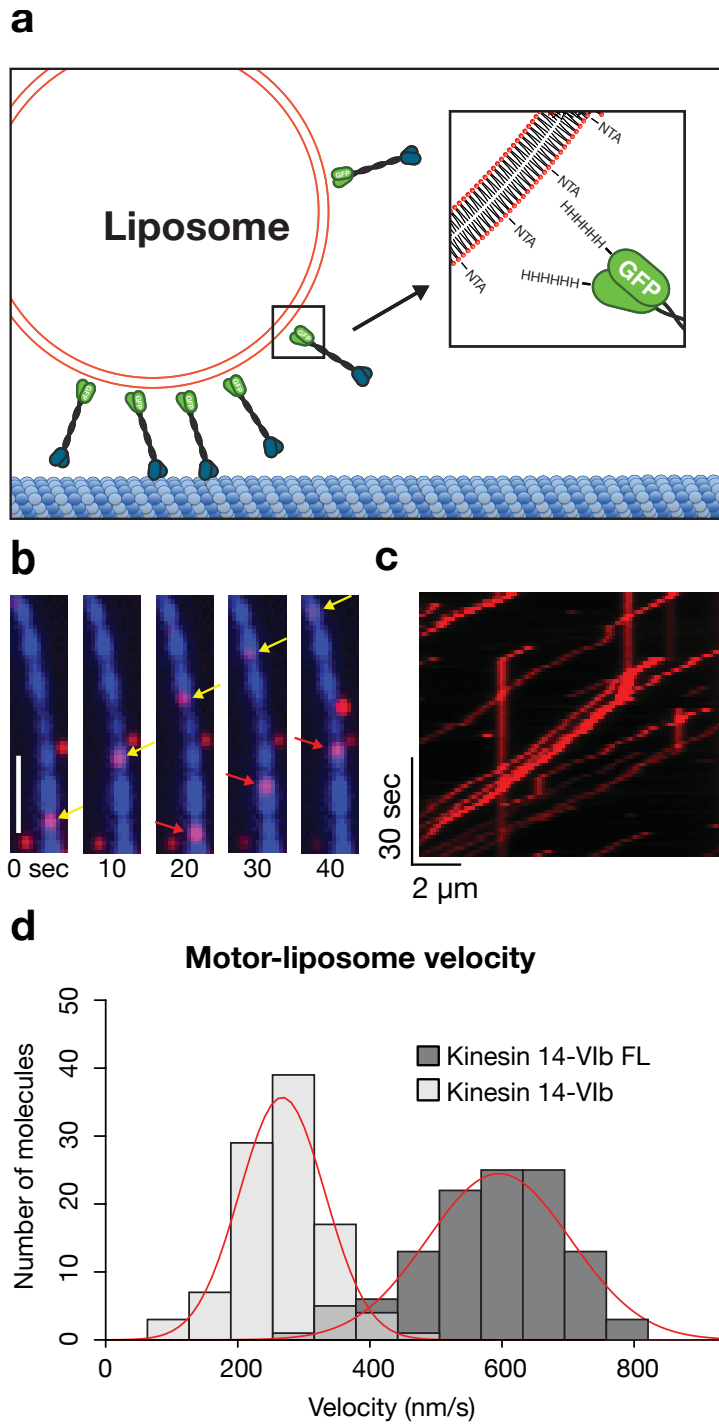


Figure 3. Kin14-VIb transports liposomes along MTs

(a) A diagram illustrating the attachment of histidine-tagged motor to Ni-NTA lipids incorporated into liposomes. (b) Transport of liposomes. Two separate motor-coated

fluorescently-labeled liposomes (red, indicated by arrows) can be seen moving along a Cy5-labeled MT (blue). Bar, 2 μm . (c) A kymograph shows long run lengths of kin14-VIb-coated liposomes. (d) Velocity histograms for liposomes coated with kin14-VIb (266 ± 69 nm/s; mean \pm SD, n = 100 particles) and kin14-VIb FL (597 ± 134 nm/s; mean \pm SD, n = 116 particles).

Finally, we tested if native kin14-VIb moves processively *in vivo*. Taking advantage of the very high frequency of homologous recombination in *P. patens*²⁹, we tagged the *Citrine* (a *GFP* variant) gene to the N-terminus of the endogenous *kin14-VIb* gene without inserting any other sequences such as selection markers; the established transgenic moss lines expressed these tagged motors under the control of the endogenous promoter and 3'UTR sequences at the native locus (Fig. S3a–c). We observed interphase cells in the protonemal tissue (Fig. 4a) using oblique illumination fluorescence microscopy; this technique has been used successfully to visualize endoplasmic MTs as well as the associated γ -tubulin-Citrine with minimum interference by autofluorescence derived from the chloroplast⁷. For Citrine-kin14-VIb, we observed discrete fluorescent punctate along the MTs, many of which showed unidirectional motility (Fig. 4b, c, Movie 4). Since only the motors and MTs were visualized by fluorescence, we could not ascertain whether or not the Citrine-kin14-VIb were bound to and moving a cargo. The mean velocity of this movement was 413 ± 18 nm/s (mean \pm SD; n = 29), which was comparable to the *in vitro* velocity, and the run length was $1.01 \pm 0.31 \mu\text{m}$ (exponential fit parameter \pm error of fit; $R^2 = 0.942$; n = 26) (Fig. 4d, e). Run lengths shorter than those that were observed in the liposome assay might reflect the fact that MT-binding of this kinesin can be negatively regulated by calmodulin binding proximal to the motor region²⁰. In some instances, we could identify the polarity of the MT along which the Citrine-kin14-VIb moved. The signals

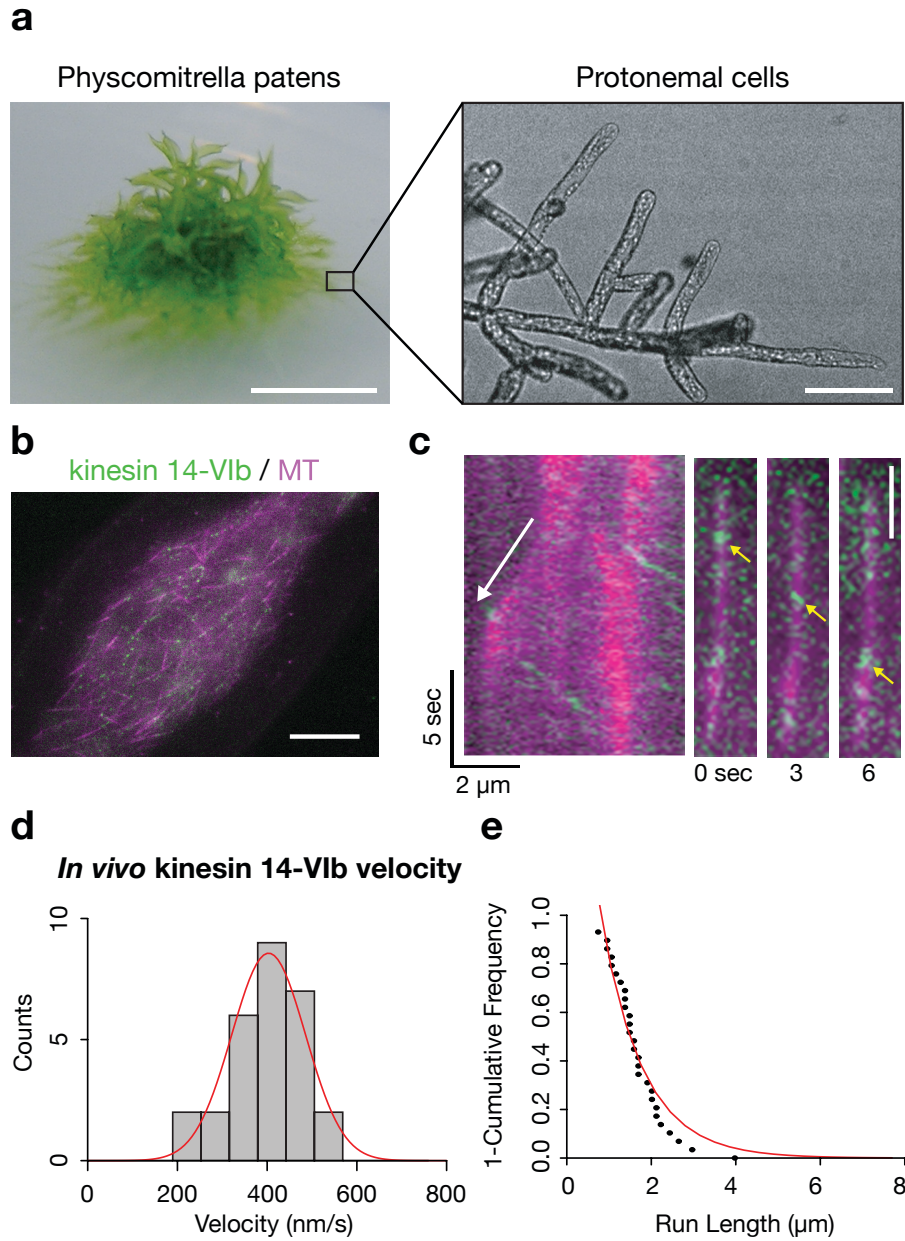


Figure 4. Minus-end-directed motility of kin14-VIb clusters *in vivo*

(a) Protonemal cells were imaged in this study. Bars, 5 mm and 100 μ m. (b) The endoplasm close to the cell cortex was observed with oblique illumination fluorescence microscopy (green; Citrine-kin14-VIb, magenta; mCherry-tubulin). Note that most of

the MTs visualized in this area are single MTs, not bundles⁷. Bar, 5 μm . (c) Citrine-kin14-VIb signals moved away from the growing plus end (white arrow in the kymograph). (Right) An example of Citrine movement (yellow arrows). Bar, 2 μm . (d) The velocity of Citrine-kin14-VIb motility ($n = 29$). Static signals were not counted. (e) 1-Cumulative frequency for run lengths of Citrine-kin14-VIb which were fit to an exponential yielding a fit parameter of $\lambda = 1.01 \pm 0.31 \mu\text{m}$ (error was determined from goodness of fit parameters; $R^2 = 0.942$, $n = 26$ particles).

28

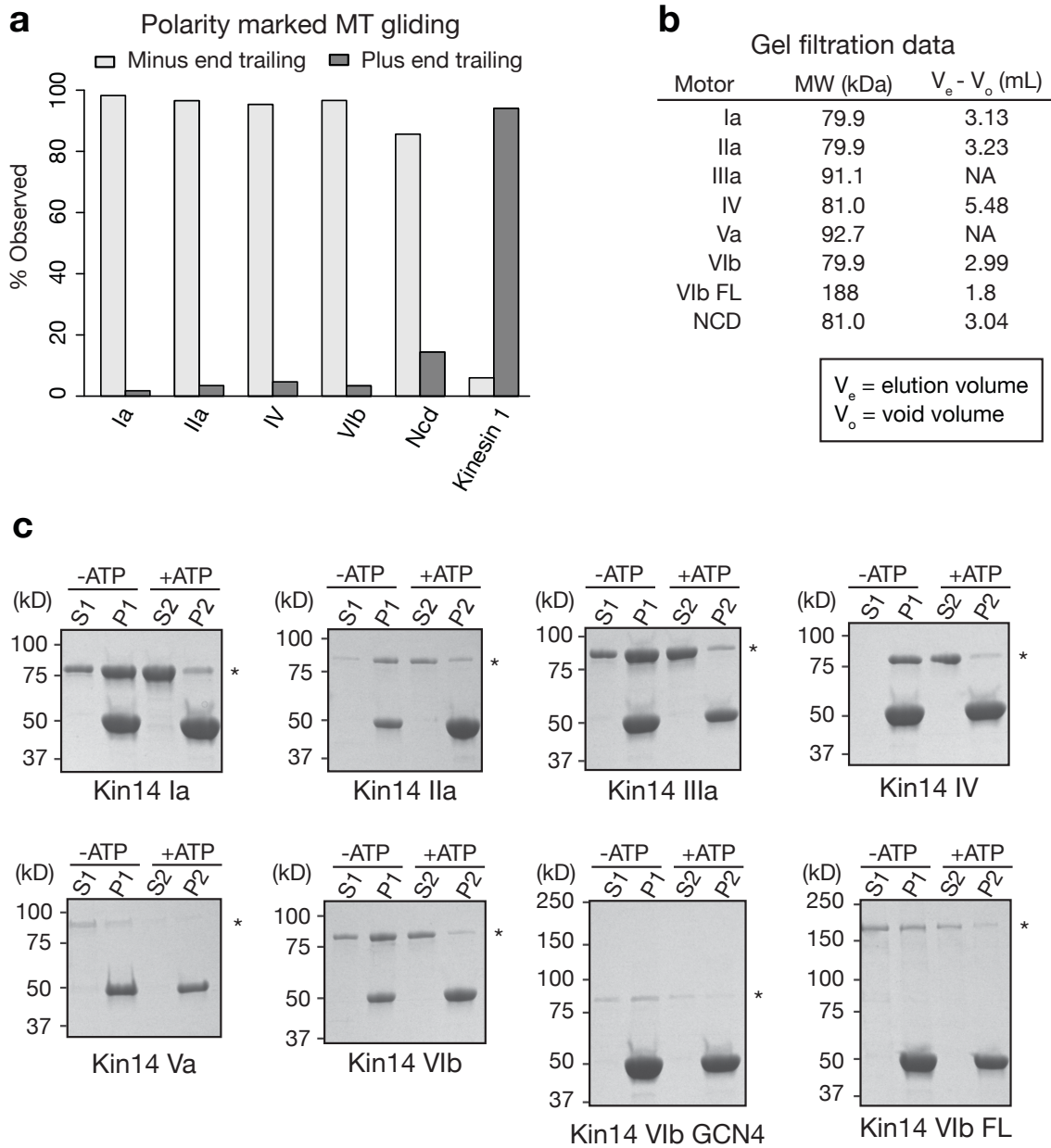
moved away from the dynamic MT plus end in all 12 cases analyzed, indicating that the Citrine-kin14-VIb moved towards minus ends (Fig. 4c). Under the same imaging condition, the fluorescence intensity of the Citrine-kin14-VIb punctae was about a half of γ -tubulin-Citrine and slightly higher than Citrine-tagged GCP4 (gamma-tubulin complex protein4) in punctae corresponding to individual γ -tubulin ring complexes (Fig. S3d; both were expressed from endogenous promoters). Assuming that 13–15 molecules of γ -tubulin and 2–4 molecules of GCP4 are present in the γ -tubulin ring complex of *P. patens* as has been estimated for animal and yeast cells^{30,31}, then it is likely that the Citrine-kin14-VIb punctae consist of more than one but relatively few dimeric kin14-VIb motor proteins. Thus, we conclude that a small number of kin14-VIb motors, clustered into a diffraction limited spot, can move processively along the MT towards minus ends in moss cells.

In conclusion, we have obtained evidence that the collective actions of as few as two non-processive kinesin-14 achieve retrograde transport *in vitro* and most likely in plant cells as well. Based on its rapid speed of transport (up to 600 nm/s; the fastest ever reported for a kinesin-14 motor) and high processivity achieved upon motor clustering, we propose that kin14-VIb acts as a cargo transport motor in plants, serving an analogous role to cytoplasmic dynein in animal and fungal cells. In the protonemal cells, we recently observed retrograde motility of newly generated MTs along the

existing MTs⁷ and MT-dependent translocation of the nucleus⁸. In the latter process, the responsible anterograde kinesin was identified and the involvement of a minus-end-directed transporter was suggested⁸. Thus, MT-dependent bidirectional transport is present in moss cells in addition to the actomyosin-based mechanism. Kin14-VIb would be a candidate retrograde motor in these processes. Previous loss-of-function and gain-of-function analyses suggested a variety of roles of kin14-VI in seed plants, such as trichome morphogenesis, pollen tube growth, organelle positioning and cell division^{17,32,33}. The versatility might be explained if kin14-VI associates with and transports various cargoes. A proof for this model would require identifying a specific cargo for kin14-VI *in vivo*.

This study also reveals similarities between kin14-VIb and other types of motors. Ncd was recently found to move with run lengths greater than 1 μm when clustered on a DNA scaffold *in vitro*³⁴. Therefore, other subgroup members of kinesin-14, even ones not involved in cargo transport, can potentially become processive *in vivo* in a similar manner to kin14-VIb. As for anterograde motors, kinesin-3 (Unc-104/KIF1), which is responsible for long-distance transport of neuronal vesicles, transports liposomes *in vitro* only after motor clustering on the liposomes surface^{35,36}. In this instance, processivity is likely achieved by promoting the association of two monomeric kinesin-3 motors into a dimer, which is the highly processive form of the motor^{35,36}. Similarly,

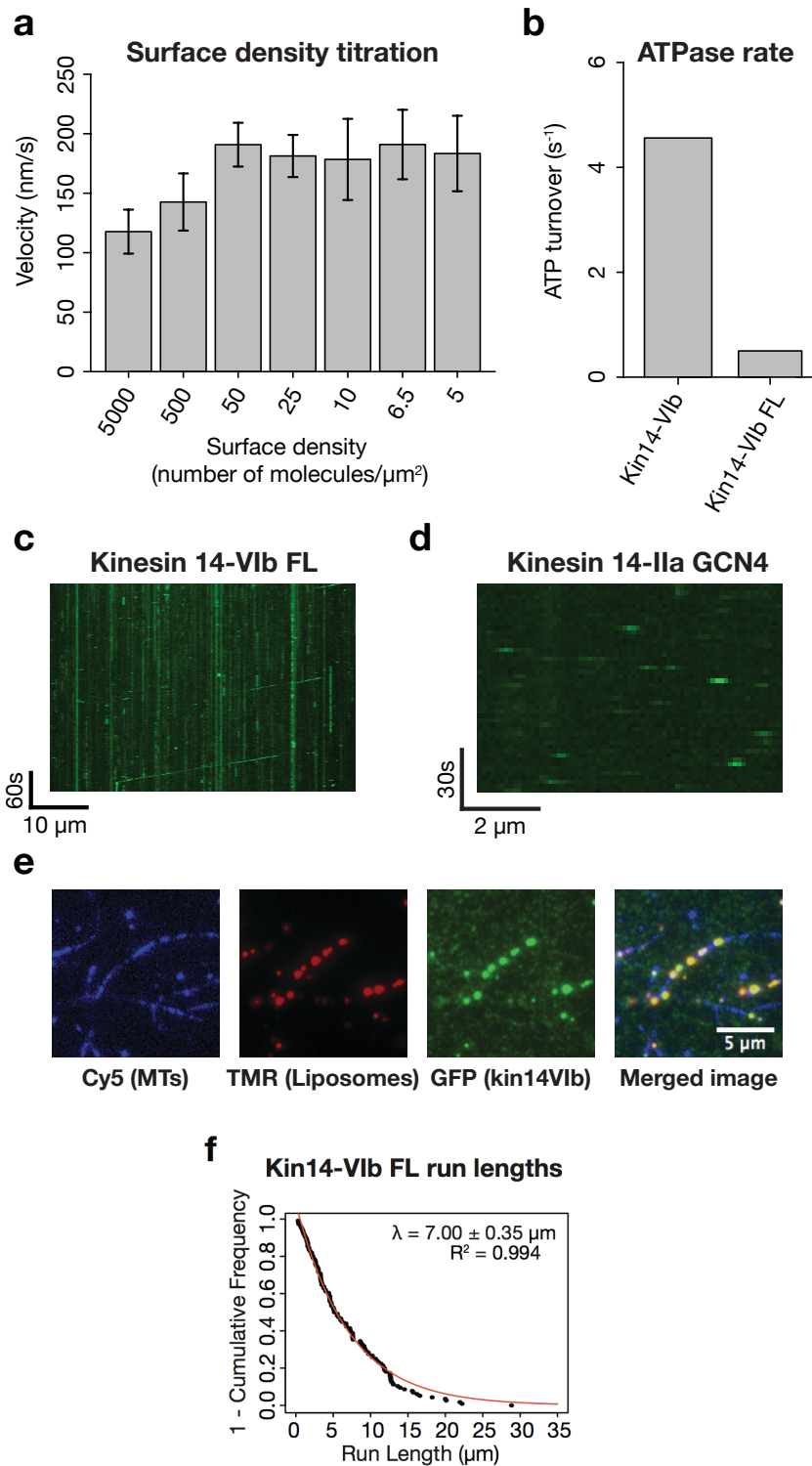
myosin VI, an actin-based motor, is monomeric and non-processive, but small clusters of this motor can efficiently produce cargo transport³⁷. Thus, the cargo-dependent clustering may be a widely utilized mechanism for cytoskeletal motors to produce long distance transport along cytoskeletal polymers.



Supplementary Figure S1. Additional *P. patens* kinesin-14 characterization

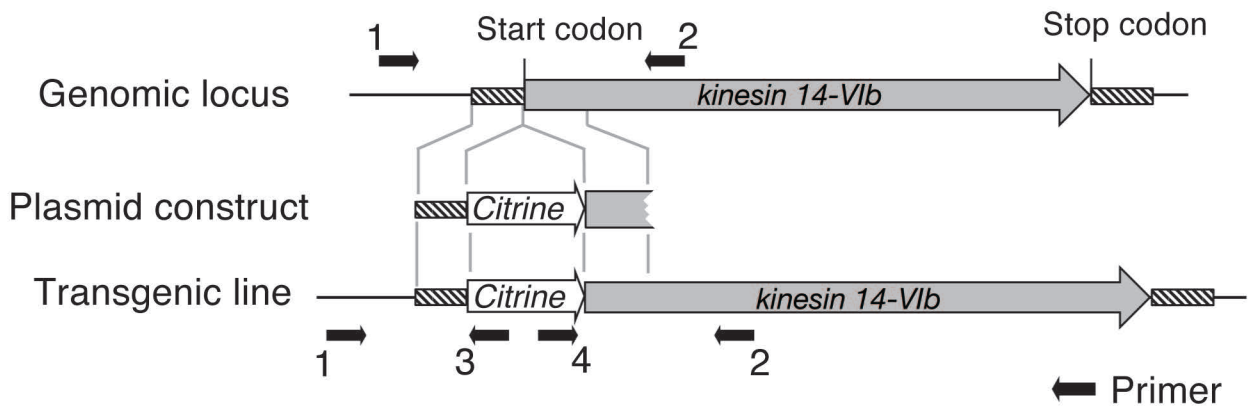
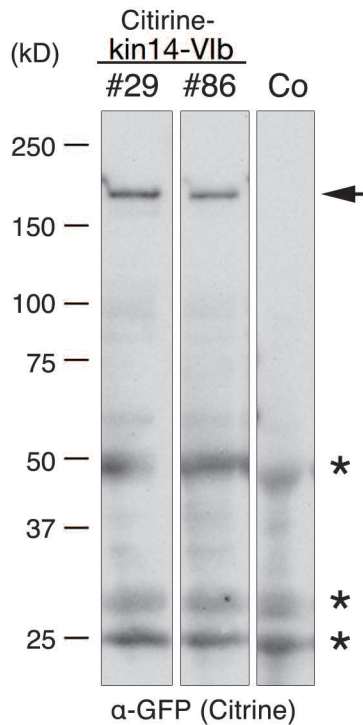
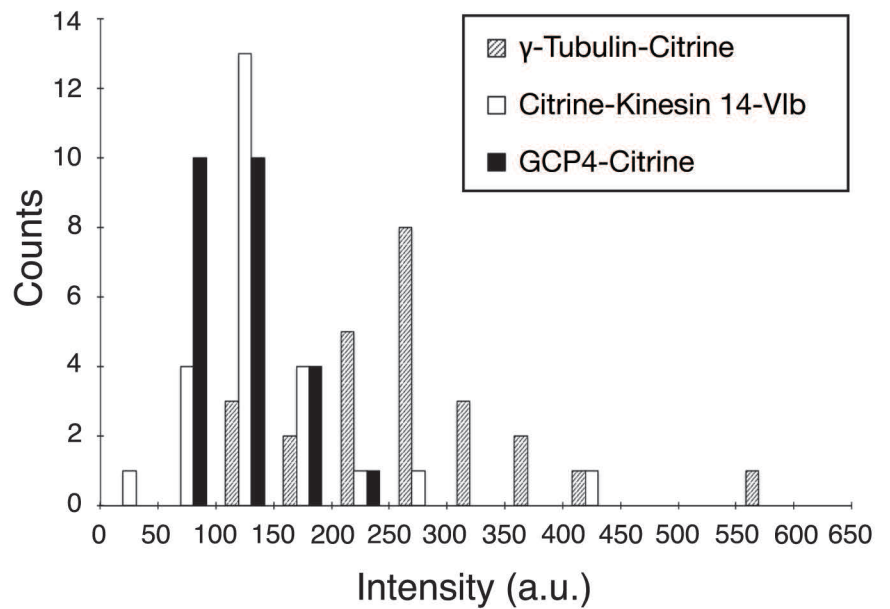
(a) The MT gliding assay using the polarity-marked MT showed that *P. patens* kinesin-14s have a retrograde polarity. Directionality of >100 polarity-marked MTs

were scored and plotted in the figure for each motor. *Drosophila* Ncd and human kinesin-1 (K560) motors served as the control minus-end-directed and plus-end-directed motors, respectively. (b) Motor proteins were run on an S200 gel filtration column and retention volumes were measured and plotted. Tabulated values are elution volume minus void volume (~8 ml for this column). (c) Representative MT bind-and-release data (see Methods) for the motors used in this study. Motors were bound to MTs in the absence of ATP and dissociated from MTs by addition of ATP. Asterisks indicate location of motor band. A peculiar case was kin14-Va, which appeared to have little interaction with MTs, which is consistent with results on the *Arabidopsis* orthologue¹⁹.



Supplementary Figure S2. Kin14-VIb full-length is non-processive on its own, but transports liposomes for long distance

(a) Gliding velocity as a function of motor surface density for kin14-VIb. For densities lower than 5 motors/ μm^2 the MTs did not glide readily and appeared diffusive. Error bars represent SDs of at least 100 motile MTs. (b) Values for the MT stimulated rate of ATP hydrolysis for both the truncated and full-length form of Kin14-VIb at a saturating MT density (20 μM). (c) A kymograph for a single molecule fluorescence assay for GFP-kin14-VIb FL (~ 1 nM). The majority of the GFP signals were not motile. However, a few processive runs were also visible (visible as diagonal lines). These particles were brighter than most of their surrounding GFP particles, indicating that they are likely small aggregates. (d) A kymograph for a single molecule fluorescence assay for GFP-kin14-IIa motor tetramerized by the GCN4 motif. Tetramerized kin14-IIa did not exhibit processive motility. (e) Bright GFP-kin14-VIb signal observed on moving liposomes due to high motor density. (f) Transport length data for liposomes coated with full-length kin14-VIb. The data points were fit to an exponential with a fit parameter of $\lambda = 7.00 \pm 0.35 \mu\text{m}$ (error is determined from goodness of fit parameters; $R^2 = 0.994$; $n = 116$ moving particles).

a**b****c****d**

Supplementary Figure S3. Establishment of the kin14-VIb replacement line

(a) Scheme of the transgenic line selection (see ⁴³ for details). The N-terminus of the endogenous *kin14-VIb* gene was tagged with the *Citrine* gene via homologous recombination. Note that no other sequences, including the selection marker gene, were integrated in this line. Arrows indicate the locations of the PCR primers used in (b). (b) Homologous recombination was confirmed by 3 sets of PCR. “Co” stands for a control line, in which the *Citrine* gene is not integrated. (c) Expression of Citrine-kin14-VIb was confirmed by immunoblotting with the anti-GFP antibody, which also recognized Citrine. Arrow indicates the band corresponding to Citrine-kin14-VIb, whereas non-specific bands are marked with asterisks. “Co” stands for a control line, in which the *Citrine* gene is not integrated. (d) Comparison of the signal intensities of Citrine-kin14-VIb, γ -tubulin-Citrine-b and GCP4-Citrine. In *P. patens*, a single GCP4 gene is present, whereas two γ -tubulin genes are expressed in protonemata (γ -tubulin-a and -b). The γ -tubulin-Citrine intensity was measured using the γ -tubulin-b-Citrine / γ -tubulin-a Δ /mCherry-tubulin line, in which all the γ -tubulin in the cells were expected to have the Citrine tag⁷. Because of the autofluorescence derived from the chloroplast, the background signals were not uniform within the cell. Therefore, we selected the same region as where the Citrine signals appeared, and measured the background signal intensity 3 frames before the Citrine signal appeared or 3 frames after the Citrine signals disappeared.

Table S1. List of PCR primers used in this study

Plasmid	Gene	5' primer	3' primer
pGG839 (pET15b)	Kin14-Ia (349–795 a.a.)	TTT <u>GCGGCCG</u> CCGGCAAGTC TGTGGCCGAGATC	AAACTCGAGCTAACTTGAACGAA TGCTCAAGG
pGG846 (pET15b)	Kin14-IIa (500–1033 a.a.)	TTT <u>GCGGCCG</u> CCGTGCAAGT GCTGAGGAATGAAC	AAAGGATCCTTACCTGGACTTAT ACTTCTCC
pGG845 (pET15b)	Kin14-IIIa (529–1070 a.a.)	TTT <u>GCGGCCG</u> CCCTGCGTGA AGATTTGTGCGCGA	AAAGGATCCTTACTCGACTACCA ACTTTTCC
pGG844 (pET15b)	Kin14-IV (90–537 a.a.)	TTT <u>GCGGCCG</u> CCTCATTGTCT TCAAGCTCCGATG	AAAGGATCCTTATGGATTGGTAG TGAATGAAG
pGG851 (pET15b)	Kin14-Va (1–556 a.a.)	TTT <u>GCGGCCG</u> CCATGGGGGA TGCAGCAGAATTGCGGT	AAAGGATCCTTATTCGTGGCTAG TAAGATCAGC
pGG840 (pET15b)	Kin14-VIb (851–1322 a.a.)	TTT <u>GCGGCCG</u> CCAGAGATGA TTTGAGGGGACG	AAAAGATCTTTAATCTGCAGTTT TGATTCC
pGG957 (pFastBacHT)	Kin14-IIa full-length	TTACTAGTGATGGATGTGGCA AGAATGG	TTGGTACCTTACCTCCAAGAGGT TGAGG
pGG960 (pFastBacHT)	Kin14-VIb full-length	TTACTAGTGATGGCCTCGGAT GCATCTCACG	TTGGTACCTTAATCTGCAGTTTTG ATTCC
pMN590 (Citrine tagging vector)	Kin14-VIb	AAAGGTACCCAAGTGTATGT CACTCTGCAATCC	AAACTCGAGTTTTATTCTCCGCCA CGACCACCC
		AAAAGTACTGTTATGGCCTCGG ATGCATCTCACGTC	AAAAGCGGCCGCCACAAGAAA AGTGTATGTCGCTGGCTG

Restriction enzyme sites are marked with underlines. *EGFP* was inserted at the NdeI site of the 6×His-containing vector pET15b (the NotI site was added at the C-terminus of the *EGFP* gene). The following linker sequences were inserted between GFP and kin14: HRYTSLYKKAGSAAA (motor constructs), QDPEFKGLRRSTSSLV (full-length constructs), or HRYTSLYKKAGSAIEDKLEEILSKLYHIENELARIKKLLGEIGGGSGGGSAAA (GCN4 tetramer construct).

Methods

Constructs

PCR primers for constructing the plasmids for protein expression and transgenic line generation are listed in Table S1. EGFP, mGFP (*in vitro*) or Citrine (*in vivo*) was attached. The information on the linker sequences is also available in the footnote of Table S1.

Protein purification

Plasmids containing the coding sequences for each of the GFP-kinesin-14 chimeras were transformed and expressed in BL21-AI cells. Expression was induced by addition of 0.2% arabinose and 0.2 μ M IPTG and were left overnight at 18°C. Cells were pelleted and harvested in lysis buffer (25 mM MOPS pH 7.0, 2 mM MgCl₂, 250 mM NaCl, 30 mM imidazole, 5 mM β -mercaptoethanol, 5% sucrose), and lysed by the EmulsiFlex homogenizer in the presence of protease inhibitors. After lysis, the extract was loaded onto a Ni-NTA column, washed with additional lysis buffer, and then eluted by increasing the imidazole concentration to 400 mM. Proteins were dialyzed for 4 h to remove imidazole and then snap frozen in liquid nitrogen and stored at -80°C.

Motility Assays

The standard assay buffer contained 25 mM MOPS pH 7.0, 75 mM KCl, 2 mM MgCl₂, 1 mM EGTA. Addition of the PCA/PCD/Trolox oxygen scavenging system³⁸ was used in all *in vitro* microscopy experiments. Purified motor proteins were subjected to a “bind-and-release” reaction, in order to select for active motors, in all motility assays used in this study. Motors were first bound to MTs for 10 min in the absence of ATP. The reaction was then layered over a 60% glycerol cushion in 1× assay buffer, supplemented with 20 μM taxol, and centrifuged at 80,000 rpm in a TLA 100 rotor for 10 min. The supernatant was discarded and the pellet was washed and resuspended in 1× assay buffer plus added KCl (to a final concentration of 150 mM) with 20 μM taxol and 5 mM ATP and left to incubate for 5 min. The solution was recentrifuged at 80,000 rpm for 10 min and the supernatant (containing motors released from the MTs with ATP) was kept on ice and used in the motility assays. Fractions at each step were analyzed by SDS-PAGE and Coomassie blue staining (Fig. S1c). For gliding assays, motors were added to a microscope slide flow chamber (~10 μL in volume) made with an untreated glass coverslip, a microscope slide and double-stick tape. After a brief incubation (2–5 min), the flow chamber was washed with assay buffer containing 1 mM casein, followed by incubation with the motility buffer containing casein, 2 mM ATP and polymerized Cy5-labeled MTs. For single molecule assays²⁷, 5 mg/ml biotin-BSA was added to a flow chamber made with acid-washed coverslips and allowed to

incubate for 2–3 min. The flow chamber was washed and supplied with 0.5 mg/ml streptavidin (another 2–3 min incubation). The flow chamber was then washed with the assay buffer containing 1 mg/ml casein, followed by a 5 min incubation with labeled MTs (10% Cy5-labeled tubulin and 10% biotin-labeled tubulin). Finally, kinesin motors in the assay buffer (with 2 mM ATP, 20 μ M taxol and 1 mg/ml casein) were added. Polarity marked MTs were made by preparing Alexa 561-labeled MT seeds, blocking the minus ends with NEM-treated tubulin, and allowing a mixture of unlabeled and Cy5-labeled tubulin (10%) to polymerize exclusively at the plus end. For the surface density titration, the same attachment chemistry was used as in the photobleaching experiments (see below). The surface density was successively titrated by preparing coverslips with the same adhered antibody concentration followed by incubating serial dilutions of GFP-motor. For very low concentrations of motor, the surface could be determined directly by counting the number of clearly visible GFP particles in a defined area. The higher surface densities (which were too high to accurately count motors individually) were estimated based on the added motor concentration and extrapolation from the surface densities that were counted directly.

In vitro microscopy instrumentation and analysis

All *in vitro* motility assays were performed at room temperature ($\sim 23^\circ\text{C}$) using total internal reflection fluorescence (TIRF) microscopy on a Nikon Eclipse Ti microscope

fitted with a 100× (1.45 NA) objective and an Andor iXON EMCCD camera. The acquisition software was Micromanager³⁹, and the analyses of velocities and run lengths were performed using FIJI. Briefly, we made kymographs for a series of motile MTs (or translocating particles) in a field of view. Velocity was then determined from these kymographs based on the acquisition parameters and the known pixel size of the microscope camera. Run lengths were also determined from kymographs of processively translocating particles. 1-Cumulative frequency distribution was plotted against run length⁴⁰ and fit to a single exponential.

Liposome preparation and motility assay

Liposomes were prepared by dissolving lipids (79.7% POPC, 10% POPS, 10% DOGS-NTA-Ni, 0.3% rhodamine PE (Avanti)) in chloroform, drying them under a constant stream of N₂ and desiccated in a vacuum for at least 1 h, and then resuspending in 1× assay buffer. To make liposomes of uniform size, the solution was extruded through polycarbonate filters with a 200 nm pore size. Motors were then added to liposomes (with at least 10-fold molar excess of motor to DOGS-NTA-Ni lipids) and incubated on ice for at least 1 h.

Photobleaching

For the photobleaching assay, HEPES pH 7.5 was substituted in the assay buffer for MOPS, because the higher pH gives a brighter GFP signal and reduces blinking. Flow chambers, made with acid-washed coverslips, were incubated with 0.1 mg/ml protein G (Sigma Chemical Co.) for ~3 min. The flow chamber was then washed followed by a 3-min incubation with an antibody against 6x histidine (0.1 mg/ml; Roche). After a wash, soluble motor was added at an appropriate concentration to achieve a surface coating of no more than ~1 particle per μm^2 . The GFP intensity was plotted in time and sequences were analyzed with custom-designed Matlab software. In Fig. 2d, ~200 traces were observed and scored according to the number of discernable bleaching events (~20% of traces were rejected due to noise).

ATPase measurement

Steady state ATP turnover was determined by a standard PK/LDH coupled assay. We diluted the standard assay buffer to 0.5x (12.5 mM MOPS pH 7.0, 37.5 mM KCl, 1 mM MgCl_2 , 0.5 mM EGTA) in order to decrease the ionic strength, which can interfere with motor-MT interactions. Final concentrations of motor were 100 nM for kin14-VIb and 225 nM for kin14-VIb FL and the MT concentration was 20 mM (which we verified was sufficiently high for maximal MT-stimulated ATP turnover). Concentrations for the other components of the assay were as follows: MgATP (2 mM), NADH (0.2 mM),

phosphoenol pyruvate (1 mM), pyruvate kinase (0.01 U), lactate dehydrogenase (0.03 U), taxol (20 mM). Absorbance at 340 nm was continuously measured in an Eppendorf Spectrophotometer (UV-Vis BioSpectrometer) to determine the rate of ATP turnover.

Moss lines

Transgenic lines were selected by the conventional PEG-mediated transformation^{41,42} with some modification (see Fig. S3a; detailed in ⁴³). Briefly, a plasmid in which the *Citrine* gene was flanked by ~1-kb 5'-UTR and N-terminal sequences of the *kin14-VIb* was constructed. After linearization, it was co-transformed into the mCherry-tubulin-expressing line with a circular plasmid with the hygromycin-resistant gene cassette. The transformants were selected by hygromycin (2 weeks), followed by transferring to the drug-free medium to allow cells to proliferate without the circular plasmid (10 d). In the end, we selected 200 transgenic lines that were no longer hygromycin resistant, and assessed the integration of *Citrine* at the N-terminus of *kin14-VIb* by PCR and immunoblotting (Fig. S3b, c). We obtained two independent Citrine-kin14-VIb replacement lines, which grew normally on the regular culture medium.

In vivo microscopy

Protonemata, the tissue containing actively dividing cells, were imaged in this study, following the method described in Ref⁷. Briefly, cells were homogenized and plated on

the cellophane-coated BCDAT agar medium for 5–7 d. Protonemal cells and 20 μ l distilled water were placed on a slide glass and covered by a coverslip. Extra water was wiped out. A TIRF microscope (Nikon Ti; 100 \times 1.49 NA lens) with a GEMINI split view (Hamamatsu) and an EMCCD camera Evolve (Roper) or iXON (DU888E; Andor) was used with oblique illumination fluorescence. The endoplasm of the sub-apical cells (or in rare cases apical cells) that was most closely located to the coverslip was in focus. Imaging was performed at 24–25°C. The microscope was controlled by Micromanager software³⁹ or Nikon's NIS-Elements. The velocity of moving particles was measured based on kymographs.

Acknowledgments

We are grateful to Stephen Ross and Lynne Chang (Nikon USA) for providing microscopes at MBL. Walter Huynh provided invaluable advice in establishing the liposome assay, and Ankur Jain assisted with the photobleaching experiment. We also thank Magdalena Bezanilla (U. Mass. Amherst) and Tomoko Nishiyama (Nagoya Univ) for help with microscopy and helpful discussion, Yuki Nakaoka for moss lines, and Momoko Nishina and Rie Inaba for technical assistance. This work was supported by the Human Frontier Science Program, the James A. and Faith Miller Memorial Fund (MBL), the Laura and Arthur Colwin Endowed Summer Research Fellowship Fund

(MBL), the TORAY Science Foundation, Grants-in-Aid for Scientific Research
(15K14540, MEXT) (G.G), and the NIH (38499; R.D.V).

References

- 1 Hirokawa, N., Noda, Y., Tanaka, Y. & Niwa, S. Kinesin superfamily motor proteins and intracellular transport. *Nat Rev Mol Cell Biol* **10**, 682-696, doi:nrm2774 [pii] 10.1038/nrm2774 (2009).
- 2 Hancock, W. O. Bidirectional cargo transport: moving beyond tug of war. *Nat Rev Mol Cell Biol* **15**, 615-628, doi:10.1038/nrm3853 (2014).
- 3 Lawrence, C. J., Morris, N. R., Meagher, R. B. & Dawe, R. K. Dyneins have run their course in plant lineage. *Traffic* **2**, 362-363 (2001).
- 4 Vale, R. D. The molecular motor toolbox for intracellular transport. *Cell* **112**, 467-480 (2003).
- 5 Shimmen, T. & Yokota, E. Cytoplasmic streaming in plants. *Curr Opin Cell Biol* **16**, 68-72, doi:10.1016/j.ceb.2003.11.009 (2004).
- 6 Cai, G. & Cresti, M. Are kinesins required for organelle trafficking in plant cells? *Front Plant Sci* **3**, 170, doi:10.3389/fpls.2012.00170 (2012).
- 7 Nakaoka, Y., Kimura, A., Tani, T. & Goshima, G. Cytoplasmic Nucleation and Atypical Branching Nucleation Generate Endoplasmic Microtubules in *Physcomitrella patens*. *Plant Cell* **27**, 228-242, doi:10.1105/tpc.114.134817 (2015).

- 8 Miki, T., Nishina, M. & Goshima, G. RNAi Screening Identifies the Armadillo Repeat-Containing Kinesins Responsible for Microtubule-Dependent Nuclear Positioning in *Physcomitrella patens*. *Plant Cell Physiol* **56**, 737-749, doi:10.1093/pcp/pcv002 (2015).
- 9 Endow, S. A. Determinants of molecular motor directionality. *Nat Cell Biol* **1**, E163-167, doi:10.1038/14113 (1999).
- 10 Mieck, C. *et al.* Non-catalytic motor domains enable processive movement and functional diversification of the kinesin-14 Kar3. *Elife* **4**, doi:10.7554/eLife.04489 (2015).
- 11 Hepperla, A. J. *et al.* Minus-end-directed Kinesin-14 motors align antiparallel microtubules to control metaphase spindle length. *Dev Cell* **31**, 61-72, doi:10.1016/j.devcel.2014.07.023 (2014).
- 12 Case, R. B., Pierce, D. W., Hom-Booher, N., Hart, C. L. & Vale, R. D. The directional preference of kinesin motors is specified by an element outside of the motor catalytic domain. *Cell* **90**, 959-966 (1997).
- 13 Hatsumi, M. & Endow, S. A. Mutants of the microtubule motor protein, nonclaret disjunctional, affect spindle structure and chromosome movement in meiosis and mitosis. *J Cell Sci* **101 (Pt 3)**, 547-559 (1992).
- 14 Goshima, G. & Vale, R. D. Cell cycle-dependent dynamics and regulation of mitotic kinesins in *Drosophila* S2 cells. *Mol Biol Cell* **16**, 3896-3907 (2005).

- 15 Shen, Z., Collatos, A. R., Bibeau, J. P., Furt, F. & Vidali, L. Phylogenetic analysis of the Kinesin superfamily from physcomitrella. *Front Plant Sci* **3**, 230, doi:10.3389/fpls.2012.00230 (2012).
- 16 Reddy, A. S. & Day, I. S. Kinesins in the Arabidopsis genome: a comparative analysis among eukaryotes. *BMC Genomics* **2**, 2 (2001).
- 17 Oppenheimer, D. G. *et al.* Essential role of a kinesin-like protein in Arabidopsis trichome morphogenesis. *Proc Natl Acad Sci U S A* **94**, 6261-6266 (1997).
- 18 Suetsugu, N. *et al.* The KAC family of kinesin-like proteins is essential for the association of chloroplasts with the plasma membrane in land plants. *Plant Cell Physiol* **53**, 1854-1865, doi:pcs133 [pii] 10.1093/pcp/pcs133 (2012).
- 19 Suetsugu, N. *et al.* Two kinesin-like proteins mediate actin-based chloroplast movement in Arabidopsis thaliana. *Proc Natl Acad Sci U S A* **107**, 8860-8865, doi:10.1073/pnas.0912773107 (2010).
- 20 Song, H., Golovkin, M., Reddy, A. S. & Endow, S. A. In vitro motility of AtKCBP, a calmodulin-binding kinesin protein of Arabidopsis. *Proc Natl Acad Sci U S A* **94**, 322-327 (1997).
- 21 Pechatnikova, E. & Taylor, E. W. Kinetic mechanism of monomeric non-claret disjunctional protein (Ncd) ATPase. *J Biol Chem* **272**, 30735-30740 (1997).

- 22 Endres, N. F., Yoshioka, C., Milligan, R. A. & Vale, R. D. A lever-arm rotation drives motility of the minus-end-directed kinesin Ncd. *Nature* **439**, 875-878, doi:10.1038/nature04320 (2006).
- 23 Verhey, K. J. & Hammond, J. W. Traffic control: regulation of kinesin motors. *Nat Rev Mol Cell Biol* **10**, 765-777, doi:nrm2782 [pii] 10.1038/nrm2782 (2009).
- 24 Harbury, P. B., Zhang, T., Kim, P. S. & Alber, T. A switch between two-, three-, and four-stranded coiled coils in GCN4 leucine zipper mutants. *Science* **262**, 1401-1407 (1993).
- 25 Ulbrich, M. H. & Isacoff, E. Y. Subunit counting in membrane-bound proteins. *Nat Methods* **4**, 319-321, doi:10.1038/nmeth1024 (2007).
- 26 Hines, K. E. Inferring subunit stoichiometry from single molecule photobleaching. *J Gen Physiol* **141**, 737-746, doi:10.1085/jgp.201310988 (2013).
- 27 Vale, R. D. *et al.* Direct observation of single kinesin molecules moving along microtubules. *Nature* **380**, 451-453, doi:10.1038/380451a0 (1996).
- 28 McKenney, R. J., Huynh, W., Tanenbaum, M. E., Bhabha, G. & Vale, R. D. Activation of cytoplasmic dynein motility by dynactin-cargo adapter complexes. *Science* **345**, 337-341, doi:10.1126/science.1254198 (2014).
- 29 Cove, D. The moss *Physcomitrella patens*. *Annu Rev Genet* **39**, 339-358, doi:10.1146/annurev.genet.39.073003.110214 (2005).

- 30 Choi, Y. K., Liu, P., Sze, S. K., Dai, C. & Qi, R. Z. CDK5RAP2 stimulates microtubule nucleation by the gamma-tubulin ring complex. *J Cell Biol* **191**, 1089-1095, doi:jcb.201007030 [pii] 10.1083/jcb.201007030 (2010).
- 31 Kollman, J. M., Polka, J. K., Zelter, A., Davis, T. N. & Agard, D. A. Microtubule nucleating gamma-TuSC assembles structures with 13-fold microtubule-like symmetry. *Nature* **466**, 879-882, doi:10.1038/nature09207 (2010).
- 32 Vos, J. W., Safadi, F., Reddy, A. S. & Hepler, P. K. The kinesin-like calmodulin binding protein is differentially involved in cell division. *Plant Cell* **12**, 979-990 (2000).
- 33 Lazzaro, M. D., Marom, E. Y. & Reddy, A. S. Polarized cell growth, organelle motility, and cytoskeletal organization in conifer pollen tube tips are regulated by KCBP, the calmodulin-binding kinesin. *Planta* **238**, 587-597, doi:10.1007/s00425-013-1919-8 (2013).
- 34 Furuta, K. *et al.* Measuring collective transport by defined numbers of processive and nonprocessive kinesin motors. *Proc Natl Acad Sci U S A* **110**, 501-506, doi:10.1073/pnas.1201390110 (2013).
- 35 Tomishige, M., Klopfenstein, D. R. & Vale, R. D. Conversion of Unc104/KIF1A kinesin into a processive motor after dimerization. *Science* **297**, 2263-2267, doi:10.1126/science.1073386 (2002).

- 36 Klopfenstein, D. R., Tomishige, M., Stuurman, N. & Vale, R. D. Role of phosphatidylinositol(4,5)bisphosphate organization in membrane transport by the Unc104 kinesin motor. *Cell* **109**, 347-358 (2002).
- 37 Sivaramakrishnan, S. & Spudich, J. A. Coupled myosin VI motors facilitate unidirectional movement on an F-actin network. *J Cell Biol* **187**, 53-60, doi:10.1083/jcb.200906133 (2009).
- 38 Aitken, C. E., Marshall, R. A. & Puglisi, J. D. An oxygen scavenging system for improvement of dye stability in single-molecule fluorescence experiments. *Biophys J* **94**, 1826-1835, doi:10.1529/biophysj.107.117689 (2008).
- 39 Edelstein, A., Amodaj, N., Hoover, K., Vale, R. & Stuurman, N. Computer control of microscopes using microManager. *Curr Protoc Mol Biol* **Chapter 14**, Unit14 20, doi:10.1002/0471142727.mb1420s92 (2010).
- 40 Bieling, P. *et al.* Reconstitution of a microtubule plus-end tracking system in vitro. *Nature* **450**, 1100-1105, doi:nature06386 [pii] 10.1038/nature06386 (2007).
- 41 Nakaoka, Y. *et al.* An inducible RNA interference system in *Physcomitrella patens* reveals a dominant role of augmin in phragmoplast microtubule generation. *Plant Cell* **24**, 1478-1493, doi:10.1105/tpc.112.098509 (2012).

- 42 Miki, T., Naito, H., Nishina, M. & Goshima, G. Endogenous localizome identifies 43 mitotic kinesins in a plant cell. *Proc Natl Acad Sci U S A* **111**, E1053-1061, doi:10.1073/pnas.1311243111 (2014).
- 43 Yamada, M., Miki, T. & Goshima, G. Imaging mitosis in the moss *Physcomitrella patens*. *Methods Mol Biol* **In press** (2015).

Chapter III
Kinesin-1 Gating

Kinesin-1 is a molecular machine that generates productive work from the free energy liberated upon hydrolyzing ATP¹. It does so in a remarkably efficient and processive manner; its high coupling ratio means that nearly every ATP hydrolysis event results in a uniform 8 nm step along the microtubule lattice^{2,3} and this cycle is repeated hundreds of times, translocating distances of over a micron, before dissociating. Single molecule studies have elucidated many of the precise details of this stepping and they generally support a model in which the two catalytic domains (also referred to as heads) cycle ATP while alternately binding and unbinding⁴ from the microtubule in a coordinated fashion. It is generally accepted that the two heads do not operate independently of one another⁵ but rather offset their catalytic cycles via an allosteric mechanism referred to *gating*. The precise mechanistic details of gating, particularly as it relates to how kinesin facilitates its processivity, have been the subject of much debate in the literature.

The neck linker (NL), a structural element important for directionality⁶ and for tethering the two heads together, is also thought to be the main conduit for gating. During the stepping process, each head alternates binding to the microtubule as a *holdfast*, preventing dissociation, while the other *tethered* head is subjected to a biased diffusional search for its next microtubule binding site⁷. Processivity necessarily requires a mechanism to prevent both heads from simultaneously dissociating from the microtubule; as one head transitions from holdfast to tethered the other transitions from tethered to holdfast and gating is thought to occur in the transient state when both heads are bound to the microtubule, referred to as a two-headed-bound (2HB) state. Studies have reported that processivity can be attenuated by increasing the length of the NL^{8,9}. Therefore models have been proposed

whereby entropic tension (or simply neck linker bias) in the 2HB state is the mode of allosteric communication. Thus two classes of gating models arise: *front head* and *rear head* gating models. An examination of rear head gating can be found in a companion paper, which will be submitted back-to-back for publication with our study. Here we focus on front head gating and in particular challenge a model that has gained prominence in the field.

In the front head gating hypothesis rearward strain (or bias) on the forward head inhibits ATP binding until the rear head detaches from the microtubule and releases the inhibition. In this study we engineered a construct designed to mimic the rearward tension in a 2HB state so that we may examine any effects on nucleotide binding directly using classical bulk fluorescence techniques¹⁰.

First, we measured the binding kinetics of mant-dATP to microtubule bound kinesin monomers. In the absence of nucleotide, kinesin forms a stable, tightly bound complex with the microtubule. When rapidly mixed with mant-dATP in stop-flow fluorometer (Figure 1A), these complexes (Figure 1B) produce signal transients which can be fitted to exponential functions (Figure 1C). The concentration dependence of the fit parameters (Figure 1E) produces two valuable pieces of information. The slope sets a lower bound on the apparent second order rate constant (k_{on}) and extrapolation to zero concentration (i.e. the y-intercept) informs us about the nucleotide dissociation rate (k_{off}). Our measurements of the Mt-K349WT complex produced kinetic parameters similar to previously reported values¹¹. For reasons that will follow later, we then proceeded to measure the mant-dATP binding kinetics of a monomer with the point mutation

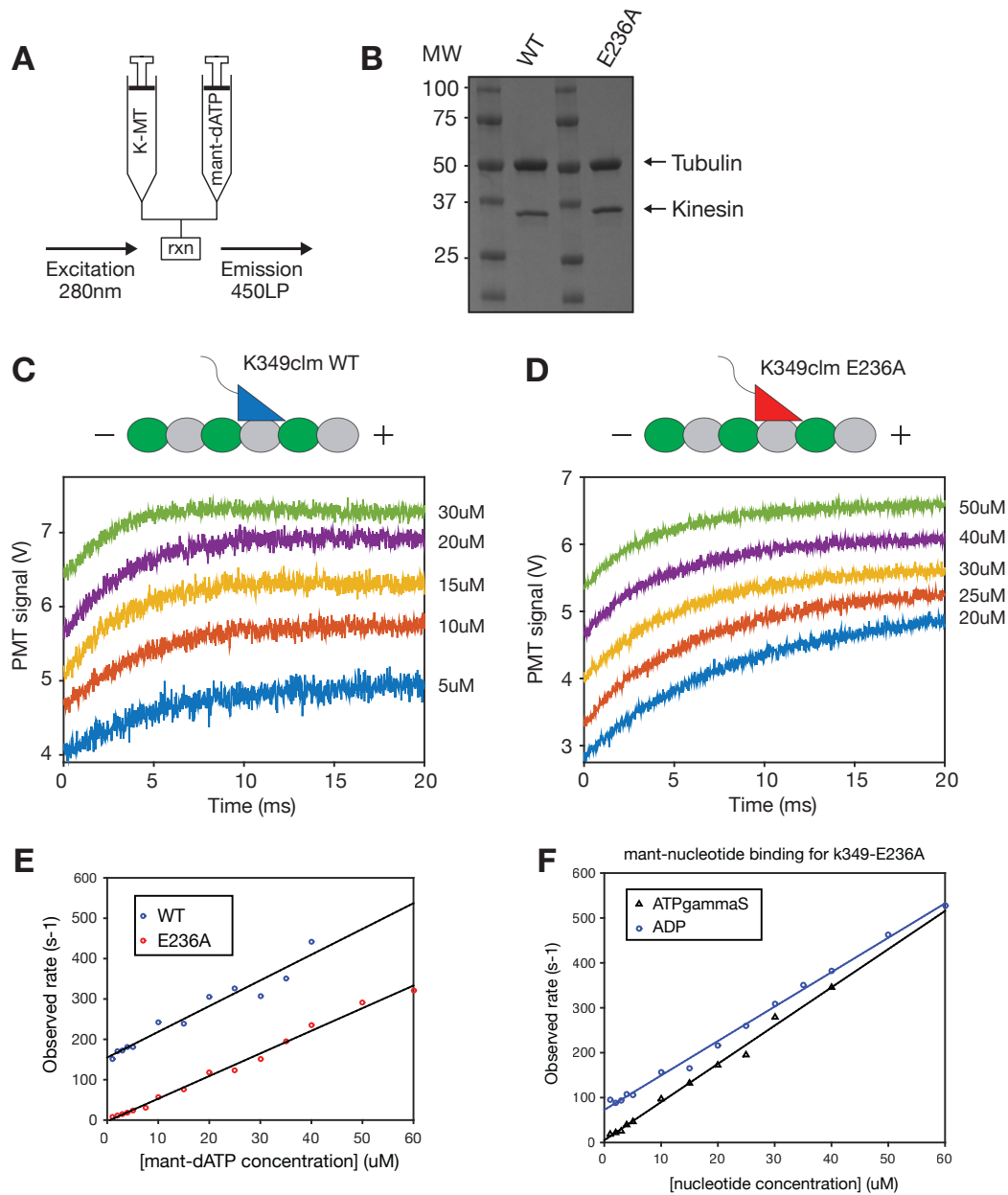


Figure 1. Mant-nucleotide binding to microtubule-bound monomeric kinesin constructs.

(A) Schematic diagram of the stop-flow apparatus. Kinesin-microtubule complexes are rapidly mixed with fluorescent nucleotide and the resulting fluorescent transients are

monitored in the reaction chamber. **(B)** A representative gel for the kinesin-microtubule complexes that are loaded into the stop-flow syringe. **(C,D)** Cartoon representations of the complexes (WT in blue and E236A in red). Representative transients from the experiment performed at different nucleotide concentrations. **(E,F)** Relationship between the exponential fit parameters and nucleotide concentration.

E236A, referred to as a rigor mutation. We measured mant-dATP binding for the Mt-K349E236A complex (Figure 1D) and observe that, while k_{on} appears to be unaffected, k_{off} is dramatically reduced. Given that the E236A mutation abrogates kinesin's ability to hydrolyze ATP, we therefore reasoned that the high k_{off} value for WT is likely due to mant-dADP dissociation after hydrolysis (Figure 4A,B) and not ATP. To follow up on this idea we measured the kinetics of other mant-nucleotides binding to the Mt-K349E236A complex. We observe that the k_{off} increases dramatically for ADP and that it falls back down with ATP γ S (Figure 1F). Thus the k_{off} value serves as a readout for the nucleotide bound in the kinesin binding pocket with ATP being more tightly bound than ADP. While there appear to be slight differences in the measured values for k_{on} , we reason that they are within the bounds of experimental error and not significantly different. Additionally, both of the monomeric constructs have unconstrained neck linkers and thus provide a measure of 'ungated' nucleotide binding. We then proceeded to design a construct that would constrain the neck linker rearward so that we could measure the relationship between rearward strain and nucleotide binding.

We chose to use the E236A mutation due to a particular trait of this mutation that was reported previously⁶; Though it cannot hydrolyze ATP, it can still bind ATP, dock its neck linker, and thus produce a single productive step. We therefore engineered and purified a heterodimer (E236A/WT) where one protomer of the dimer contains the E236A mutation and the other is WT (see methods). We reasoned that in the presence of ATP, such a construct would be *loaded* onto the microtubule such a way that it becomes trapped in a 2HB state in which the rigor mutation head trails the WT head. First we measured the steady state ATPase rate of this construct and compared it to a WT monomer. Since the rigor mutation is catalytically inactive we can be sure

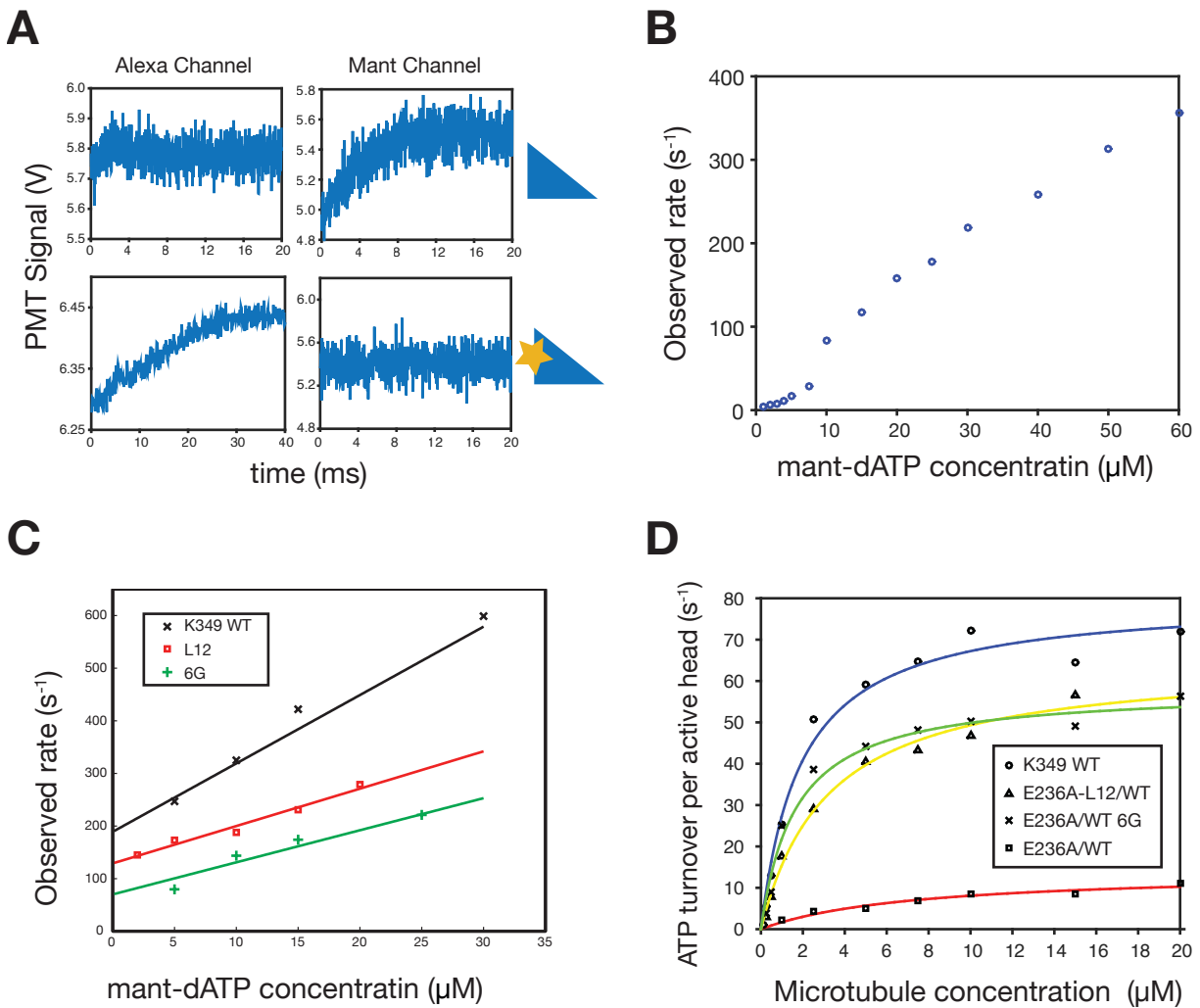


Figure 2. Kinesin heterodimer kinetic measurements

(A) Representative mant-dATP binding traces from both unlabeled and Alexa-488 labeled kinesin monomer. Without the FRET label the signal is observed in the mant channel. With labeled kinesin we observe a signal in the Alexa channel and that the

mant signal is quenched. A heterodimer labeled in this way will allow for distinguishing binding to labeled vs unlabeled head. **(A)** Mant-dATP binding the unlabeled WT head of the heterodimer (front head). S-shape is present at around 7 μM . **(C)** Mant-dATP binding to the 6G and L12 heterodimers as compared to a WT monomer. **(D)** Steady-state microtubule stimulated ATPase rate of the various constructs used in this study.

E236A, referred to as a rigor mutation. We measured mant-dATP binding for the Mt-K349E236A complex (Figure 1D) and observe that, while k_{on} appears to be unaffected, k_{off} is dramatically reduced. Given that the E236A mutation abrogates kinesin's ability to hydrolyze ATP, we therefore reasoned that the high k_{off} value for WT is likely due to mant-dADP dissociation after hydrolysis (Figure 4A,B) and not ATP. To follow up on this idea we measured the kinetics of other mant-nucleotides binding to the Mt-K349E236A complex. We observe that the k_{off} increases dramatically for ADP and that it falls back down with ATP γ S (Figure 1F). Thus the k_{off} value serves as a readout for the nucleotide bound in the kinesin binding pocket with ATP being more tightly bound than ADP. While there appear to be slight differences in the measured values for k_{on} , we reason that they are within the bounds of experimental error and not significantly different. Additionally, both of the monomeric constructs have unconstrained neck linkers and thus provide a measure of 'ungated' nucleotide binding. We then proceeded to design a construct that would constrain the neck linker rearward so that we could measure the relationship between rearward strain and nucleotide binding.

We chose to use the E236A mutation due to a particular trait of this mutation that was reported previously⁶; Though it cannot hydrolyze ATP, it can still bind ATP, dock its neck linker, and thus produce a single productive step. We therefore engineered and purified a heterodimer (E236A/WT) where one protomer of the dimer contains the E236A mutation and the other is WT (see methods). We reasoned that in the presence of ATP, such a construct would be *loaded* onto the microtubule such a way that it becomes trapped in a 2HB state in which the rigor mutation head trails the WT head. First we measured the steady state ATPase rate of this construct and compared it to a WT monomer. Since the rigor mutation is catalytically inactive we can be sure

Table 1: Steady state ATPase

Construct	k_{cat} (s ⁻¹)	K_m (μM)
K349clm WT	80 ± 9	1.9 ± 0.8
K349clm E236A	N.A.	N.A.
K490clm WT	43 ± 8	8.7 ± 4.0
E236A/WT	14	6
E236A-L12/WT	65 ± 6	3.2 ± 1.0
E236A/WT (6G)	59 ± 6	1.7 ± 0.7

that all ATPase turnover with the heterodimer is due to the WT head. If front head gating exists (and it has been reported that ATP binding is inhibited 100-fold in this configuration¹²) then we would expect a dramatic decrease in ATPase activity. Instead what we observe is about a six-fold decrease in ATPase turnover (Figure 2, squares). To relieve the effects of strain and rescue WT behavior we designed two additional heterodimeric constructs. In the first construct, we added an additional 12 amino acids, 6 glycines to each protomer thus we name it E236A/WT (6G). In the second, we include with the rigor mutation a set of mutations known as L12 which impair its ability to bind the microtubule. Thus one construct relieves strain by extending the tether length between the heads and the other does so by preventing the formation of a 2HB state. In both cases the ATPase rate increased and rescued that of WT. These results are also summarized in Table 1. Clearly there is some inhibition but not to the extent we might have expected for a front-head-gating model. However, we reasoned that the steady state assay might not be as sensitive to any effect and thus we proceeded to measure the pre-steady state binding kinetics for mant-dATP.

Our first attempts to measure mant-dATP on the heterodimer produced signal transients that were difficult to interpret (data not shown). We suspected, however, that the problem might be due to mant-dATP binding both heads (front and back). So we therefore devised a FRET based strategy to distinguish binding events between the two heads. Based on the kinesin structure¹³, we screened a series of locations adjacent to the nucleotide binding pocket where we could introduce a cysteine for subsequent maleimide labeling. We found that the combination of H100C mutation labeled with an Alexa-488 dye produced a robust FRET signal (Figure 2A). Surprisingly we also found that the FRET probe completely quenched the mant fluorescence signal (see methods). Therefore, just as we can selectively mutate each protomer in a

homodimer we can also selectively introduce a FRET probe in either the WT head or the E236A head. This strategy affords us the opportunity to distinguish binding events between the two heads; any signal in the mant channel is due to the unlabeled head (WT), while signal from the Alexa channel is due to FRET from labeled head (E236A). Armed with the ability to distinguish binding between the front and rear head, we proceed to measure the mant-dATP binding kinetics for the heterodimer (Figure 2B). The shape of the front head curve has a peculiar transition at low nucleotide concentration (we will refer to it as an S-shape) which was previously observed in a similar context¹⁴. The original interpretation of the cause of the S-shape was problematic, however, and our strategy allows us to draw a different conclusion which will be addressed by future experiments (still pending). Disregarding the points in the vicinity of the transition, the slopes of the curve at low mant-dATP concentration and at high mant-dATP concentration do not appear to be drastically different than the slopes measured on monomers. This further supports the notion that k_{on} is unaffected by choice nucleotide. Additionally the slope of the curve starting from a mant-dATP concentration of about 10 μ M on is not that dissimilar to what we measured for the monomer (i.e. with an unconstrained NL and thus ‘ungated’). This suggests that k_{on} for mant-dATP binding is not dramatically affected by rearward strain and we therefore conclude that k_{on} is neither affected by strain nor by nucleotide (ATP, ADP, ATP γ S).

Exact interpretation of k_{off} for the heterodimer is more difficult but it does *not* support the current gating hypothesis. If ATP binding is dramatically diminished due to strain then it can happen in one of two ways. Either k_{on} is dramatically reduced or k_{off} is dramatically increased (or perhaps a combination of both). Here we observe neither effect and in fact k_{off} appears to drop significantly – i.e. it binds nucleotide more tightly. We then followed up with mant-dATP binding

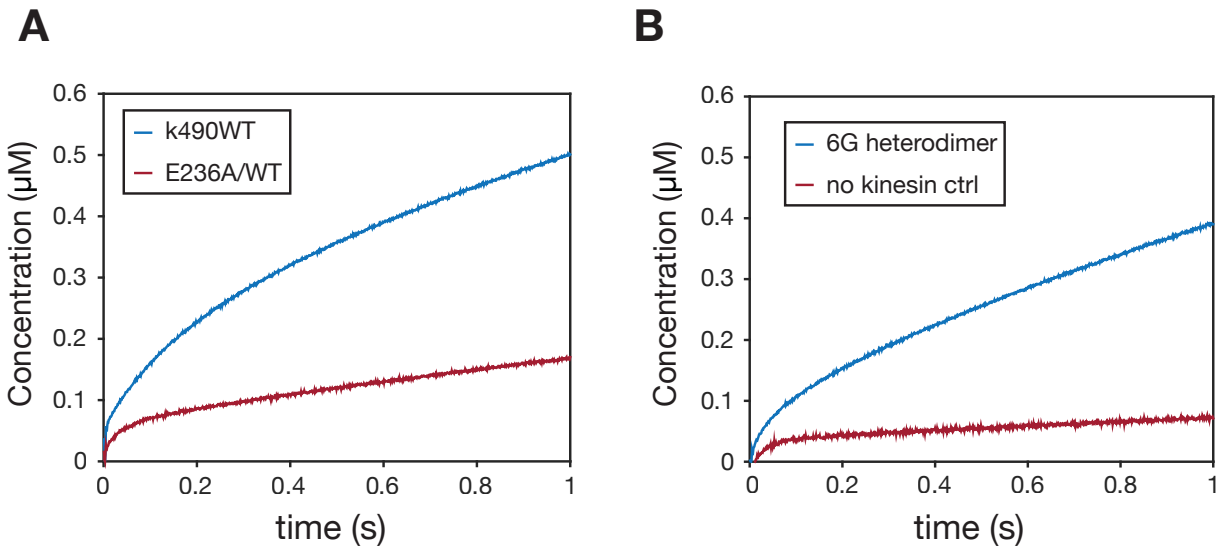


Figure 3. Phosphate release kinetics

(A) Comparison of PBP measurement on kinesin homodimer vs heterodimer. The size of the burst phase in the heterodimer appears to be significantly reduced. The linear phase shows a decrease in steady state activity. (B) The extended neck linker construct appears to slightly recover the burst phase of WT. A no nucleotide control shows that there might be some mixing artifacts and thus the experiment needs to be repeated.

measurements for the heterodimer rescue mutants (6G and L12 with the added FRET probe to distinguish front/rear head binding). We again find that k_{on} is not dramatically different than all other nucleotide binding measurements. k_{off} also exhibits some downward trend, consistent with the steady state observation that the rescue mutants do not completely rescue the WT behavior - likely due to some diffusional constraint on the neck linker with respect to the monomer. But the effect of relieving strain on these mutants does appear to shift k_{off} back towards WT. Additionally, the values for k_{off} range continuously from $\sim 0 \text{ s}^{-1}$ to $\sim 150 \text{ s}^{-1}$ and this suggests that the effect of front head gating is due to rearward strain not simply NL bias. We conclude that, while rear tension does gate kinesin somehow, it does not do so at the level of ATP binding and also that gating is sensitive to tension.

It is possible that gating occurs downstream of nucleotide binding. To investigate this we proceeded to measure the kinetics of phosphate release to compare the differences between the WT and heterodimers. Using phosphate binding protein (PBP)¹⁵ we can measure the pre-steady state rate of phosphate release in real time. Kinesin has previously been shown to exhibit burst kinetics¹⁶. Surprisingly we find that the heterodimer's burst phase is absent (Figure 3A) as compared to WT. When we assay a rescue mutant (E236A/WT 6G) the burst phase returns (Figure 3B). These results are still preliminary, however, and are in the process of being repeated and verified.

But if the disappearance of the burst phase holds up in further experiments it would suggest that the rate-limiting step in the kinesin cycle may be shifted as a result of tension. If this is in fact the case, then it is possible that ATP hydrolysis or phosphate release is what is affected by rearward

strain. Further experiments are required to answer definitively, however. These experiments are on going but, as of the writing of this dissertation, are not yet completed. However the conclusion that our evidence does not support front head gating model is a big step advancement in the field.

References

1. Vale, R. D., Reese, T. S. & Sheetz, M. P. Identification of a novel force-generating protein, kinesin, involved in microtubule-based motility. *Cell* **42**, 39–50 (1985).
2. Hua, W., Young, E. C., Fleming, M. L. & Gelles, J. Coupling of kinesin steps to ATP hydrolysis. *Nature* **388**, 390–393 (1997).
3. Schnitzer, M. J. & Block, S. M. Kinesin hydrolyses one ATP per 8-nm step. *Nature* **388**, 386–390 (1997).
4. Yildiz, A., Tomishige, M., Vale, R. D. & Selvin, P. R. Kinesin Walks Hand-Over-Hand. *Science* **303**, 676–678 (2004).
5. Hackney, D. D. Evidence for alternating head catalysis by kinesin during microtubule-stimulated ATP hydrolysis. *Proc. Natl. Acad. Sci.* **91**, 6865–6869 (1994).
6. Rice, S. *et al.* A structural change in the kinesin motor protein that drives motility. *Nature* **402**, 778–784 (1999).
7. Carter, N. J. & Cross, R. A. Mechanics of the kinesin step. *Nature* **435**, 308–312 (2005).
8. Hackney, D. D., Stock, M. F., Moore, J. & Patterson, R. A. Modulation of Kinesin Half-Site ADP Release and Kinetic Processivity by a Spacer between the Head Groups†. *Biochemistry (Mosc.)* **42**, 12011–12018 (2003).
9. Yildiz, A., Tomishige, M., Gennerich, A. & Vale, R. D. Intramolecular Strain Coordinates Kinesin Stepping Behavior along Microtubules. *Cell* **134**, 1030–1041 (2008).

10. Gilbert, S. P. & Mackey, A. T. Kinetics: A Tool to Study Molecular Motors. *Methods* **22**, 337–354 (2000).
11. Ma, Y.-Z. & Taylor, E. W. Kinetic Mechanism of a Monomeric Kinesin Construct. *J. Biol. Chem.* **272**, 717–723 (1997).
12. Rosenfeld, S. S., Fordyce, P. M., Jefferson, G. M., King, P. H. & Block, S. M. Stepping and Stretching HOW KINESIN USES INTERNAL STRAIN TO WALK PROCESSIVELY. *J. Biol. Chem.* **278**, 18550–18556 (2003).
13. Jon Kull, F., Sablin, E. P., Lau, R., Fletterick, R. J. & Vale, R. D. Crystal structure of the kinesin motor domain reveals a structural similarity to myosin. *Nature* **380**, 550–555 (1996).
14. Ma, Y.-Z. & Taylor, E. W. Interacting Head Mechanism of Microtubule-Kinesin ATPase. *J. Biol. Chem.* **272**, 724–730 (1997).
15. Brune, M., Hunter, J. L., Corrie, J. E. T. & Webb, M. R. Direct, Real-Time Measurement of Rapid Inorganic Phosphate Release Using a Novel Fluorescent Probe and Its Application to Actomyosin Subfragment 1 ATPase. *Biochemistry (Mosc.)* **33**, 8262–8271 (1994).
16. Gilbert, S. P., Webb, M. R., Brune, M. & Johnson, K. A. Pathway of processive ATP hydrolysis by kinesin. *Nature* **373**, 671–676 (1995).
17. Gilbert, S. P., Moyer, M. L. & Johnson, K. A. Alternating Site Mechanism of the Kinesin ATPase. *Biochemistry (Mosc.)* **37**, 792–799 (1998).

Methods

Protein purification

Plasmids (pET-17b for monomers and pRSFDuet for heterodimers) containing the coding sequences for each of the kinesin constructs were transformed and expressed in BL21-DE3 cells. Expression was induced by addition of 0.2 μ M IPTG and were left overnight at 18°C. Cells were pelleted and harvested in lysis buffer (25 mM HEPES pH 7.5, 2 mM MgCl₂, 250 mM KCl, 30 mM imidazole, 0.5 mM TCEP, 0.1 mM ATP), and lysed by the EmulsiFlex homogenizer in the presence of protease inhibitors. After lysis, the extract was loaded onto a Ni-NTA column, washed with additional lysis buffer, and then eluted by increasing the imidazole concentration to 400 mM. Monomeric (and also homodimeric) proteins were then passed over an S200 Gel filtration column containing GF buffer (25mM PIPES pH 6.8, 2 mM MgCl₂, 100 mM KCl, 0.1 mM ATP, 10% glycerol). Heterodimeric constructs were subjected to an additional round of affinity purification, via Streptactin resin, to properly select for heterodimeric motors. The elution from the nickel column was diluted 2-fold (to reduce imidazole concentration) and was incubated with Streptactin resin for 1 hour. The beads were then washed with ST buffer (25 mM HEPES pH 7.5, 2 mM MgCl₂, 100 mM KCl, 0.1 mM ATP) and eluted with ST buffer containing 2.5 mM desthiobiotin. Proteins were then incubated with 5-fold molar excess Alexa-488 C5 maleimide for at least 30 min. The reaction was quenched with 10mM DTT and then the protein was passed over a

gel filtration column containing GF buffer. Protein concentration and labeling efficiency was determined followed by snap freezing in liquid N₂ and stored at -80°C.

Steady state ATPase measurements

Steady state ATP turnover was determined by a standard PK/LDH coupled assay. We diluted the standard assay buffer to 0.5x (12.5 mM MOPS pH 7.0, 37.5 mM KCl, 1 mM MgCl₂, 0.5 mM EGTA) in order to decrease the ionic strength, which can interfere with motor-MT interactions. Final concentrations of motor were 100 nM for kin14-VIb and 225 nM for kin14-VIb FL and the MT concentration was 20 mM (which we verified was sufficiently high for maximal MT-stimulated ATP turnover). Concentrations for the other components of the assay were as follows: MgATP (2 mM), NADH (0.2 mM), phosphoenol pyruvate (1 mM), pyruvate kinase (0.01 U), lactate dehydrogenase (0.03 U), taxol (20 mM). Absorbance at 340 nm was continuously measured in an Eppendorf Spectrophotometer (UV-Vis BioSpectrometer) to determine the rate of ATP turnover.

Pre-steady state kinetics

Kinesin was loaded onto microtubules in the following way. Monomers (10 μM) were incubated with microtubules (25 μM) in the absence of nucleotide for approximately 5 minutes. And then spun over a glycerol cushion (4x volume) at 80K rpm for 10 minutes. The pellet was then resuspended in 1x assay buffer (BRB25 + 10mM NaCl +

20 μ M Taxol). To determine protein concentration the K-MT resuspension was run on a gel with a BSA standard to measure the kinesin concentration (target for stop flow reactions were 1 μ M after mixing). Heterodimers were treated similarly except that the initial incubation with microtubules was done in the presence of 1 mM ATP. Stop flow experiments were performed on a Kintek SF-2004 stop flow apparatus. K-MT complexes were rapidly mixed with various concentrations of mant-nucleotides. Excitation wavelength for mant-nucleotide binding experiments was 280 nm and emission was measured using a 450/50 bandpass filter. For FRET measurements, the excitation wavelength was 345 nm and emission was measured using a ET510 longpass filter.

Chapter IV
In Conclusion

We have seen that nature has evolved two different approaches to processivity. As there are other known mechanisms in the literature as well, it is likely that the different approaches confer different advantages over one another. Individually, the kin-14VIb motor is not processive but can be induced to be. Perhaps this is so that processivity can only be accessed when necessary, i.e. turned on and off like a switch unlike kinesin-1 which is constitutively processive with a different regulatory machinery. As our knowledge of the kinesin 14 motors in chapter II is just beginning, there are countless future experiments that one could conceive. Rather than follow up on a project that is so open ended, we will focus the remainder of this discussion on the kinesin-1 gating mechanism which has proved elusive for so long.

The main conclusion concerning gating is that the current front head gating (FHG) model is wrong and needs to be revised. It is clear that ATP occupancy is *not* inhibited by rearward strain (or bias) on the neck linker (NL). However, it is clear that something *is* occurring as a result of rearward strain and the problem now becomes how to generate a model which reconciles the new results with previous studies. But before I begin to summarize our findings it is imperative to adopt a consistent naming convention that will facilitate a more coherent discussion. I will use the term *binding* to

refer exclusively to kinesin-microtubule binding. For nucleotide-kinesin interactions I will refer to *affinity*, *nucleotide occupancy*, or the specific rate constants (k_{on} , k_{off}). For example, there is no ambiguity in the following statement: “ADP occupied kinesin is generally assumed to be weakly bound to the microtubule”. Dimeric motors can bind the microtubule with both heads, in which case I will refer to this configuration as a *two-headed-bound* (2HB) state, where it is clear what *front* and *rear* head mean. Alternatively, a dimer may bind the microtubule with one head thus the microtubule-bound head is the *holdfast* head and the other is the *tethered* head. So the classic half-site inhibited complex from Hackney’s 1994 paper¹ is simply a one headed bound dimer with an Apo holdfast head and an ADP occupied tethered head. Now, on to the discussion.

The data strongly suggests a relationship between strain and the rate of nucleotide dissociation (k_{off}). Differences in k_{on} appear to be within the bounds of experimental error; this is true for both WT and E236A monomers as well as the three different nucleotides (ATP, ADP and ATPyS). Therefore let us assume that k_{on} is unaffected and that any gating, at the level of nucleotide affinity, manifests itself exclusively via k_{off} . This is, in fact, a more parsimonious model than the previous FHG model for two reasons. First, there is precedent as it has been clear for some time that the microtubule stimulates ATP hydrolysis by dramatically increasing the off rate of ADP².

Second, alternately modulating k_{on} from high to low would likely require a large structural rearrangement of the nucleotide cleft of the motor domain, presumably at a high energetic cost. It would mean that as the tethered head makes contact with the microtubule, stimulating ADP release, rearward tension on the head is so great that it prevents subsequent ATP occupancy, even though it is structurally similar to an ADP which had just occupied the cleft. And, given that ATP is present at very high concentration ($\sim 5\text{mM}$) it would not be surprising to learn that this parameter is difficult to regulate. Additionally, nowhere in the literature does k_{on} ever appear to be significantly different than about $\sim 5 \text{ uM}^{-1} \text{ s}^{-1}$ for either nucleotide free kinesin or microtubule bound kinesin. In short, it seems likely that the value of k_{on} is set by the ATP concentration of the cell and that k_{off} is an evolutionarily easier dial to modulate, given that kinesin is already known to use it.

The other big takeaway from the data is that, while affinity does change in response to tension it does so counter to what we would expect from the FHG hypothesis. The effect of rearward tension is to increase affinity, not decrease it. Before addressing this discrepancy, it is helpful to recall the original studies^{3,4} that motivated the FHG model in the first place, which have since been revisited⁵. These studies relied on a particular optical trapping geometry to measure the microtubule unbinding rates of monomeric and dimeric kinesin in the presence of different nucleotide concentrations. The

conclusions of these three studies relied on the same observation that there is an asymmetry in the unbinding rates that occurs in the presence of ADP (not ATP); rear loading in the presence of ADP causes kinesin to bind tighter to the microtubule. This is consistent with the observation that, in the presence of ADP, kinesin steps more rapidly towards the plus end with forward load than it does towards the minus end with rearward load⁶. The experimental approaches in these early studies were sensitive to both weak and strong unbinding events and focused on the distribution of weak vs strong changes upon varying the nucleotide concentration. The logic for the original interpretation proceeded as follows. A *strong* unbinding event was interpreted as microtubule-bound Apo kinesin that had detached. Alternatively, a *weak* unbinding event was interpreted as the detachment of microtubule-bound ADP-occupied kinesin. Stated more simply, if the force to detach the motor was small then it was assumed that the kinesin was ADP occupied. If it was high then it was assumed that the kinesin was Apo. But we have shown that that tension does not affect k_{on} and the trend we observe for k_{off} suggests that rearward strain would increase the likelihood of being occupied with ADP. Thus there is a contradiction with these assumptions and the conclusion that follows is problematic. The conclusion was that *more kinesin were tightly bound because rearward strain reduced the affinity for ADP*, i.e. the increase was due to a higher population of Apo kinesins. This statement is clearly incorrect, in light of our findings.

This assumption (inhibited ADP occupancy) has motivated all future work on FHG and, in fact, the only other attempt⁷ to measure directly any effect on nucleotide affinity also relied on the kinetics of ADP binding (not ATP). First, let me propose a model to replace it, after which I will explain my reasoning.

Model: ADP occupied kinesin binds to the microtubule in an equilibrium of both a strongly bound and weakly bound states. In the absence of any strain based gating, the equilibrium favors the weak binding state. The effect of *rearward* strain on the NL serves to shift the equilibrium towards the strong binding state. The effect of *forward* strain on the NL serves to shift the equilibrium towards the weak binding state (Figure 1A).

This replacement of the current model will make many disparate findings fall in line. In our study, we found that rearward tension drops the k_{off} of the measured nucleotide, thereby increasing affinity. The experimental conditions that give rise to a low k_{off} (E236A mutant, ATPyS) are states that are generally considered to be strong binding states. ADP can recover a high k_{off} for the E236A mutant, which suggests that the affinity of the nucleotide is modulated not by the nucleotide itself but the conformation

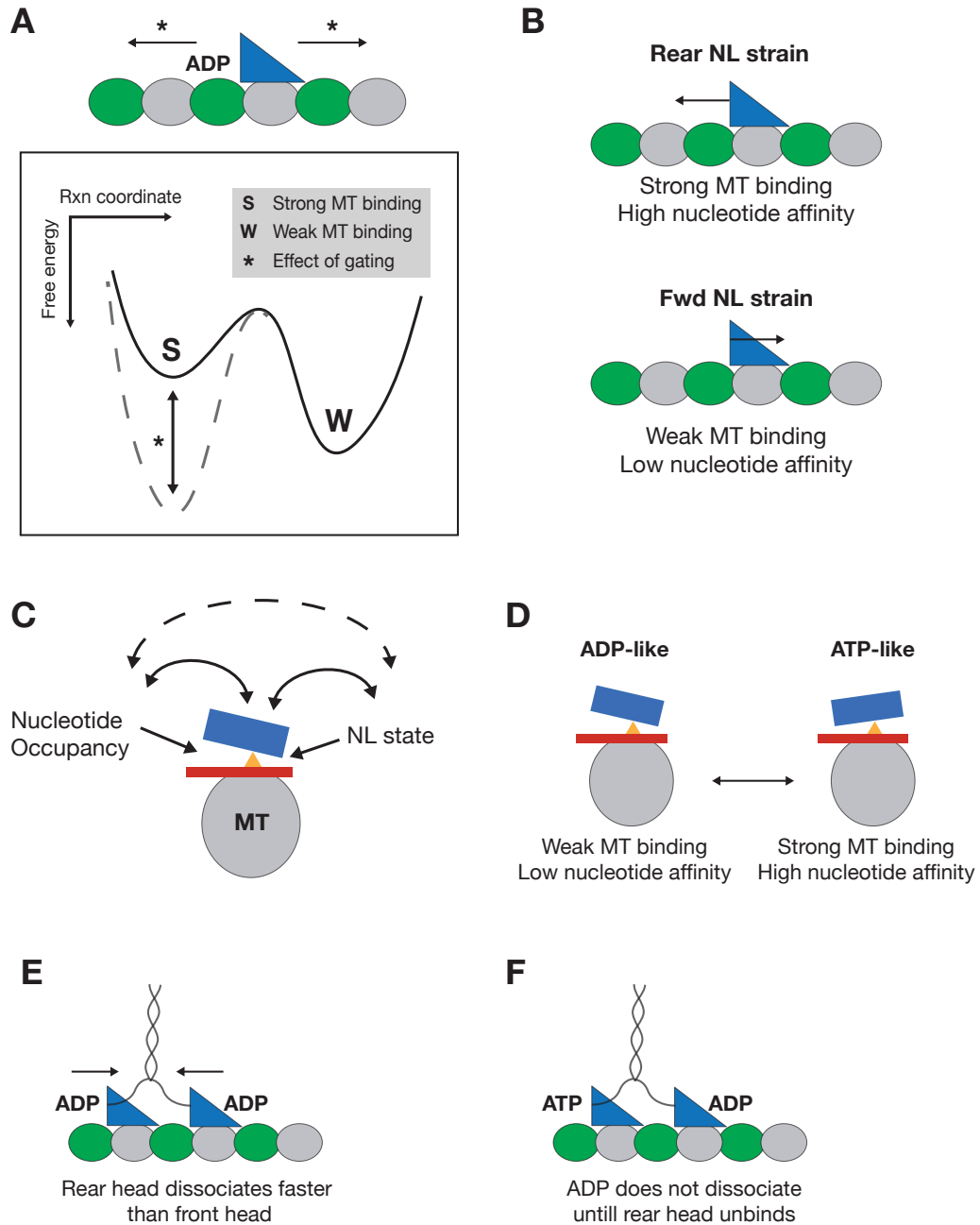


Figure 1. Model for kinesin front head gating mechanism

(A) ADP occupied microtubule-bound kinesin can exist in an equilibrium of both weak and strong binding to the microtubule. The effect of gating either preserves the

equilibrium (forward strain) or shifts the binding towards the strong binding state (rearward strain). **(B)** In the model rearward strain leads to strong microtubule binding and high nucleotide affinity. Forward strain promotes weak microtubule binding and low nucleotide affinity. **(C)** Seesaw mechanism. The tilt of the catalytic core (blue) relative to the switch II helix (red) can be influenced by both nucleotide occupancy and/or neck linker state (solid arrows). The old model (dashed arrows) connected nucleotide occupancy to neck linker state directly (and vice versa). **(D)** The new model is that nucleotide affinity is an indirect effect of catalytic core tilt. Tilt in the catalytic core ultimately influences whether kinesin is strongly (ATP-like) or weakly (ADP-like) bound to the microtubule. **(E)** Mode of kinesin dissociation that front head gating model was thought to inhibit. **(F)** A successful kinesin step under the new model.

of the nucleotide cleft of the motor. Therefore, the value of k_{off} serves as a readout for whether kinesin is strongly or weakly bound to the microtubule and this can be modulated by forward or rearward strain on the NL (Figure 1B).

If this is in fact the case, consider a 2HB state. It was originally thought that ADP occupied in both the front and rear head in a 2HB state would lead to dissociation. But the unbinding asymmetry in the presence of ADP suggest that this state would not be a problem; the ADP bound head in the rear would dissociate more quickly than the forward head (Figure 1E). It was often assumed that this state is the main mode of dissociation and that any gating mechanism existed mainly to prevent this state from occurring. But our results in light of previous findings suggests that this state is not problematic. A successful forward step, therefore, perhaps looks more like it does in figure 1F (previously it was assumed that the front head was Apo after a successful step).

Recent structural work supports this mechanism as a plausible model. Detailed information about how kinesin binds to the microtubule has generally been lacking, due to the difficulty crystalizing the microtubule-kinesin complexes, but recent advances in EM techniques have offered a closer look. An intriguing model to emerge from these studies^{8,9} is called a ‘seesaw mechanism’ based on the idea that the catalytic

core of kinesin appears to tilt with respect to the switch II loop that binds the microtubule. Tilting is a balance between effects from the nucleotide and effects from the neck linker (Figure 1C). In this model (without going into too much detail) the tilting of the catalytic core switches from “ADP-like” orientations to “ATP-like” orientations (Figure 1D). The tilt of the catalytic core is what ultimately determines MT binding affinity. It is possible that rearward strain on kinesin (regardless of what nucleotide is occupying the cleft) is tilting the core towards the ATP-like conformation which would manifest itself in tight microtubule binding and low nucleotide affinity – as we observe. Also, I suspect that ADP, lacking a gamma phosphate that would facilitate formation of the phosphate tube¹⁰, is the only nucleotide that easily can accommodate both ATP-like and ADP-like conformations – which would explain why previous gating studies relied exclusively on ADP as a proxy for ATP. ADP is the nucleotide that gave rise to the unbinding asymmetry³⁻⁵ not AMP-PNP and not Apo. ATP does display some asymmetry but it is hard to de-convolute whether the effect is occurring when the nucleotide cleft is occupied with ATP or ADP, since hydrolysis is so fast.

Experiments are underway to test the model proposed here and will be submitted for publication soon.

References

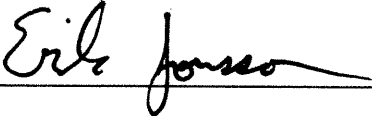
1. Hackney, D. D. Evidence for alternating head catalysis by kinesin during microtubule-stimulated ATP hydrolysis. *Proc. Natl. Acad. Sci.* **91**, 6865–6869 (1994).
2. Hackney, D. D. Kinesin ATPase: rate-limiting ADP release. *Proc. Natl. Acad. Sci.* **85**, 6314–6318 (1988).
3. Uemura, S. & Ishiwata, S. Loading direction regulates the affinity of ADP for kinesin. *Nat. Struct. Mol. Biol.* **10**, 308–311 (2003).
4. Uemura, S. *et al.* Kinesin–microtubule binding depends on both nucleotide state and loading direction. *Proc. Natl. Acad. Sci.* **99**, 5977–5981 (2002).
5. Dogan, M. Y., Can, S., Cleary, F. B., Purde, V. & Yildiz, A. Kinesin’s Front Head Is Gated by the Backward Orientation of Its Neck Linker. *Cell Rep.* **10**, 1967–1973 (2015).
6. Yildiz, A., Tomishige, M., Gennerich, A. & Vale, R. D. Intramolecular Strain Coordinates Kinesin Stepping Behavior along Microtubules. *Cell* **134**, 1030–1041 (2008).
7. Rosenfeld, S. S., Fordyce, P. M., Jefferson, G. M., King, P. H. & Block, S. M. Stepping and Stretching HOW KINESIN USES INTERNAL STRAIN TO WALK PROCESSIVELY. *J. Biol. Chem.* **278**, 18550–18556 (2003).

8. Sindelar, C. V. A seesaw model for intermolecular gating in the kinesin motor protein. *Biophys. Rev.* **3**, 85–100 (2011).
9. Sindelar, C. V. & Downing, K. H. An atomic-level mechanism for activation of the kinesin molecular motors. *Proc. Natl. Acad. Sci.* **107**, 4111–4116 (2010).
10. Shang, Z. *et al.* High-resolution structures of kinesin on microtubules provide a basis for nucleotide-gated force generation. *eLife* e04686 (2014).
doi:10.7554/eLife.04686

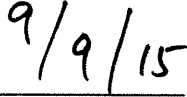
Publishing Agreement

It is the policy of the University to encourage the distribution of all theses, dissertations, and manuscripts. Copies of all UCSF theses, dissertations, and manuscripts will be routed to the library via the Graduate Division. The library will make all theses, dissertations, and manuscripts accessible to the public and will preserve these to the best of their abilities, in perpetuity.

I hereby grant permission to the Graduate Division of the University of California, San Francisco to release copies of my thesis, dissertation, or manuscript to the Campus Library to provide access and preservation, in whole or in part, in perpetuity.



Author Signature



Date